Research Square

Preprints are preliminary reports that have not undergone peer review.
They should not be considered conclusive, used to inform clinical practice,
or referenced by the media as validated information.

Biological Activity of Irradiated Amniotic Membrane Extract with Zinc Oxide Nanoparticles in the Treatment of Atopic Dermatitis-Associated Bacteria: In Vitro Study

Waleed A. Nemr

wnemr@hotmail.com

National Centre for Radiation Research and Technology (NCRRT), Egyptian Atomic Energy Authority (EAEA)

Inas I. Raafat

National Centre for Radiation Research and Technology (NCRRT), Egyptian Atomic Energy Authority (EAEA)

Nashwa K. Radwan

National Centre for Radiation Research and Technology (NCRRT), Egyptian Atomic Energy Authority (EAEA)

Neveen Abdelaziz

National Centre for Radiation Research and Technology (NCRRT), Egyptian Atomic Energy Authority (EAEA)

Eman Araby

National Centre for Radiation Research and Technology (NCRRT), Egyptian Atomic Energy Authority (EAEA)

Article

Keywords: Antibiotic resistance, antimicrobial peptide, biocompatibility, clinical visibility

Posted Date: November 2nd, 2026

DOI: https://doi.org/10.21203/rs.3.rs-11255320/v1

License: This work is licensed under a Creative Commons Attribution 4.0 International License.
Read Full License

Additional Declarations: No competing interests reported.

Biological Activity of Irradiated Amniotic Membrane Extract with Zinc Oxide Nanoparticles in the Treatment of Atopic Dermatitis- Associated Bacteria: *In Vitro Study*

Waleed Nemr [(1)]; Inas I. Raafat[(1)] ; Nashwa K. Radwan [(2)] ; Neveen Abdelaziz[(1)]; Eman Araby[(1)]

(1) Radiation Microbiology Department, National Centre for Radiation Research and Technology (NCRRT), Egyptian Atomic Energy Authority (EAEA), Cairo, Egypt.

(2) Radiation Health Research Department, National Centre for Radiation Research and Technology (NCRRT), Egyptian Atomic Energy Authority (EAEA), Cairo, Egypt.

Corresponding author: Waleed A. Nemr

Email: wnemr@hotmail.com

ORCID: 0000-0001-8465-0497

Key words:

Antibiotic resistance, antimicrobial peptide, biocompatibility, clinical visibility

Biological Activity of Irradiated Amniotic Membrane Extract with Zinc Oxide Nanoparticles in the Treatment of Atopic Dermatitis- Associated Bacteria: *In Vitro Study*

Abstract

Atopic dermatitis (AD) hand lesions present a complex clinical challenge characterized by persistent microbial dysbiosis, severe cutaneous inflammation, unmitigated oxidative stress, and epidermal barrier breakdown. This study evaluated the therapeutic potential, clinical feasibility, and safety limits of a novel nano-bio-formulation combining Zinc Oxide Nanoparticles (ηZnO) and Irradiated Amniotic Membrane Extract (IAME) against multidrug-resistant (MDR) bacteria isolated directly from active AD hand lesions. Forty-five clinical isolates belonging to five predominant biofilm-forming species—*Staphylococcus aureus*, *Staphylococcus epidermidis*, *Staphylococcus hominis*, *Staphylococcus warneri*, and *Kocuria rosea*—were isolated and characterized. The 1:1 ηZnO + IAME co-formulation demonstrated potent, multi-targeted efficacy by eradicating established bacterial biofilms (up to 92% biomass reduction across $n = 33$ multidrug-resistant isolates), suppressing heat-induced bovine serum albumin protein denaturation ($IC_{50} = 81.65\ \mu$L/mL), and exhibiting superior DPPH free-radical scavenging capacity ($IC_{50} = 15.65\ \mu$L/mL) comparable to standard Ascorbic Acid ($IC_{50} = 17.14\ \mu$L/mL). Cell culture evaluations on human dermal fibroblasts demonstrated that co-administering IAME attenuated ηZnO-induced cytotoxicity by $> 80\%$, maintaining cell viability near 90%. Crucially, both the pharmacological IC_{50} values and the antimicrobial minimum inhibitory concentrations (MIC = 12.5--25 μL/mL) were substantially lower than the co-formulation's cytotoxicity IC_{50} threshold. This highlighting a safe, highly biocompatible, non-steroidal topical candidate capable of breaking the chronic infection–inflammation–oxidative stress cycle and restoring epidermal homeostasis in AD hand lesions.

Introduction

Over the past few decades, the global prevalence of AD has been significantly increased. According to the Global Burden of Diseases, Injuries, and Risk Factors Study (GBD) 2021, there were an estimated 129 million (95% uncertainty interval: 124–134 million) individuals with AD worldwide in 2021 **[1]**, around 20% of children, and 5% of adults **[2]**. Microbial imbalance (dysbiosis) in the skin is one of reasons leading to AD pathogenesis in immunologically compromised patients. This chronic disease is the most common form of eczema, arises from immune system dysregulation, as characterized by intense itching (pruritus), rash, and relapsing inflammatory skin **[3]**.

Cutaneous dysbiosis disrupts normal skin microflora, aggravating both inflammation and barrier breakdown in atopic dermatitis (AD) lesions **[4]**. In particular, increased colonization by *Staphylococcus aureus* plays a key role in disease severity. The presence of inflammation led to the emergence of additional bacterial strains and altered the relative proportions of bacterial species that are normally present on healthy skin **[5]**. So, the understanding of this dysbiosis is crucial for developing targeted therapies that address the root causes of the disease rather than just its symptoms.

The global dissemination of multidrug-resistant (MDR) bacterial pathogens represents one of the most critical threats to modern medicine, severely complicating the management of chronic inflammatory dermatoses **[6,7]**. Among these conditions, atopic dermatitis (AD) is uniquely vulnerable. The hallmark pathophysiological features of AD—including structural breakdown of the epidermal barrier, reduced endogenous antimicrobial peptide synthesis, and immune dysregulation—create a permissive microenvironment for microbial colonization **[8,9]**. *Staphylococcus aureus* colonizes up to 90% of patients with active AD lesions, frequently evolving into refractory multidrug-resistant strains, notably methicillin-resistant *S. aureus* (MRSA) **[5,10]**. The proliferation of MDR pathogens not only precipitates secondary superinfections but also perpetuates chronic cutaneous inflammation through the continuous secretion of enterotoxins, proteases, and pore-forming cytotoxins, driving a self-sustaining cycle of disease exacerbation and tissue damage **[11,12]**.

Consequently, conventional therapeutic paradigms—historically dependent on topical and systemic antibiotics alongside anti-inflammatory corticosteroids—are increasingly failing due to widespread antimicrobial resistance and the risk of microbiome dysbiosis **[13,14]**. Repeated exposure to standard antibiotics selects for resistant phenotypes and destabilizes the commensal skin microflora, while prolonged topical corticosteroid application carries significant risks of epidermal atrophy, systemic absorption, and rebound flares **[15]**. This growing therapeutic bottleneck highlights an urgent biomedical priority: developing novel, non-traditional antimicrobial strategies—such as cell-free stem cell derivatives, antimicrobial peptides, endolysins, and target-specific biologics—capable of selectively eradicating MDR pathogens, neutralizing bacterial virulence factors, and enhancing dermal re-epithelialization without driving further resistance or damaging the host skin microenvironment **[16,17]**.

Zinc oxide nanoparticles (ηZnO) have emerged as powerful inorganic antimicrobial agents capable of overcoming multi-drug resistance and eradicating recalcitrant bacterial biofilms **[18,19]**. The broad-spectrum antibacterial activity of ηZnO is governed by a multi-modal mechanism of action, primarily driven by the localized release of zinc ions (Zn^{2+}), direct electrostatic adhesion and mechanical disruption of bacterial cell walls, and the continuous generation of surface reactive oxygen species (ROS) such as hydroxyl radicals and hydrogen peroxide under physiological conditions **[20,21]**. In the context of Atopic Dermatitis (AD) hand lesions, where opportunistic *Staphylococcus* species form dense extracellular polymeric substance (EPS) matrices that restrict conventional antibiotic penetration, the nanostructured core of ηZnO acts as a physical penetrator, destabilizing the structural integrity of the biofilm and disrupting bacterial membrane potentials **[22,23]**. However, the clinical translational utility of ηZnO monotherapy remains severely constrained by its inherent concentration-dependent cytotoxicity toward mammalian cells **[20]**. High local concentrations of bare ηZnO nanoparticles can trigger intracellular oxidative stress, mitochondrial damage, and apoptosis in healthy human dermal fibroblasts, creating a narrow therapeutic safety window that limits its direct application on compromised skin barrier surfaces **[20,21]**.

Gamma radiation is an effective sterilization method for natural and biomedical materials, as it inactivates bacteria, viruses, and fungi without heat or chemicals. It has been successfully applied to natural polymers and bioactive extracts, preserving their physical and biological properties while ensuring microbial safety. This makes gamma irradiation suitable for preparing and sterilizing natural products for therapeutic, pharmaceutical, and regenerative medicine applications **[24]**.

Natural bioproducts such as the secretome from infection-stimulated amniotic epithelial cells provide a rich source of antimicrobial proteins and cutaneous growth factors **[25]**. Accordingly, the present study aimed to characterize the bacterial profile associated with atopic dermatitis (AD) hand lesions and evaluate its susceptibility to infection-conditioned amniotic membrane extract (IAME) alone and in combination with ηZnO. This dual approach seeks to develop a novel therapeutic formulation capable of disrupting the chronic "infection–inflammation–oxidative stress" cycle and promoting epidermal barrier restoration in AD hand lesions.

Materials and Methods

Patients and study legality

The research protocol for this study was reviewed and approved by the Research Ethics Committee of the National Center for Radiation Research and Technology (REC-NCRRT; IRB 00011179), Egyptian Atomic Energy Authority (EAEA), under approval number (F/5H/24). All procedures involving human participants (with informed consent) were conducted in strict accordance with the ethical standards of the Declaration of Helsinki (**2013**) **[26]**.

Detailed information about the research procedures was explained to patients (with AD lesion in their hands) in the outpatient clinic of the Faculty of Medicine for Girls, Al Azhar University, and accordingly some of them signed the informed consent to participate this study. Patients were excluded if they had received antibiotics or topical medications at the target AD lesion within one week prior to sample collection. The total comprised participants achieved 30 patients having AD hand lesions last for at least 6 months before sampling; 18 females and 12 males with ages ranging from 25 to 56 years.

Sample collection

Microbiological samples were collected by swabbing each AD skin lesion (in hands) using a sterile cotton swab after immersing it into sterile 0.9% Sodium Chloride saline solution. The wet swab was used to rub against the targeted skin surface, with continuous rotation for at least 15 sec. The collected swabs were transported (under cooling) immediately to the Bacteria and Viruses lab, NCRRT, for further microbiological assessments.

Isolation and identification of MDRs

Under strict aseptic conditions, swab samples were used to inoculate Tryptone Soya Agar medium (TSA; Oxoid), supplemented with 10 mg/L Amphotericin B (Gibco) to prevent fungal contamination, followed by incubation at 35 °C for 24 hours. Individual bacterial colonies were purified by streak-plating on fresh TSA plates. Representative single colonies were transferred to Tryptone Soya Broth (TSB) to obtain pure liquid cultures.

Antimicrobial resistance profiling was evaluated on Mueller–Hinton Agar (MHA, 90 mm) using the disk diffusion technique in accordance with CLSI (2007) guidelines **[27]**. Inoculated MHA surfaces were air-dried for 10 min prior to applying the following antibiotic disks (Oxoid): methicillin (ME, 5 µg), vancomycin (VA, 30 µg), amoxicillin/clavulanic acid (AMC, 30 µg), tobramycin (TOB, 10 µg), gentamicin (CN, 10 µg), sulfamethoxazole–trimethoprim (SXT, 25 µg), nalidixic acid (NA, 30 µg), imipenem (IPM, 10 µg), and ciprofloxacin (CIP, 5 µg). After 24 hours incubation at 35 °C, zone diameters were recorded. Multidrug-resistant (MDR) phenotypes were identified based on resistance to ≥ 5 of the 9 tested agents ($\geq 55.56\%$ resistance). Colonies growing adjacent to disks with no or minimal inhibition zones were isolated with a sterile loop to maintain purified stocks of each MDR isolate. The percentage of antibiotics resistance was calculated using the following formula:

$$\text{Antibiotic Resistance (\%)} = \left(\frac{\text{Count of negative inhibition zone discs}}{\text{Total number of the tested antibiotics}=9}\right) \times 100$$

All MDR bacterial isolates were subjected for some discriminative morphological and biochemical tests including; Gram staining, cultivation on selective Mannitol salt agar and Baird-Paker agar media **[28],** Coagulase **[29],** Catalase **[30],** Trehalose fermentation **[31]**, and Modified Oxidase (Microdase test) **[31]**.

Accordingly, MDR bacterial isolates that showed similar morphological and biochemical characteristics were represented by those having greater antibiotic-resistance value (maximum 4 isolates of each group). These selected isolates were subjected for further confirmatory identification test using Matrix-Assisted Laser Desorption/ionization-Time of Flight (MALDI-TOF) LT3 instrument (SAI, UK). Briefly, a single colony was taken from a fresh solid culture plate and spotted on a specific stainless-steel plate. Then, 1 ul of 50% α-Cyano-4-hydroxycinnamic acid (HCCA) matrix (47.5% Acetonitrile (CAN), 2.5% Trifluoroacetic acid (TFA) in water) was mixed with the colony and left to dry under laminar air flow. Mass spectra were obtained using linear mode and extracting positive ions with an accelerating voltage of 25 kV. The identification was performed and matched to the BactoScreen database. Scores above 0.8 are considered a match for both Genus and species, as per the software used.

Preparation of HAM antibacterial extract

The human amniotic membrane was obtained and proceeded according to the methodology published previously **[32]**. The amniochorionic tissue was dissected from placenta of elective cesarean section deliveries, following thorough screening for transmissible infectious agents; in collaboration with Al-Galaa Maternity Hospital, Cairo, Egypt. Human tissue sampling was performed in strict accordance with the ethical standards of the Declaration of Helsinki and relevant institutional guidelines and regulations. The experimental protocols for obtaining, processing, and utilizing human amniotic tissues were formally reviewed and approved by the Ethics Committee of the National Center for Radiation Research and Technology (REC-NCRRT; IRB 00011179), Egyptian Atomic Energy Authority (EAEA), under approval number (F/5H/24).

The purified amnion was trypsinized for 1 hour by 50 ml of 0.025% trypsin (Sigma-Aldrich) in Minimal Essential Medium (MEM). Cellular viability was checked by Trypan blue staining **[25]**. Samples represented viability less than 80% were discarded from the experiment. Valid samples were divided by sterile scissors into small pieces (ranged from 3-5 grams/piece) and incubated over night at 37ºC under shaking (with rotation speed = 30 rpm) in trypsin solution (each 1 gram of amnion was digested by 5 ml Trypsin solution) for completing the digestion reaction. The induction of HAM cells to secret antimicrobial proteins was done according to the strategy published by **Nemr et al (2017) [25]**. Briefly, 10^4 CFU of the isolated bacterial species (after inactivation by the minimal dose of gamma irradiation that causes growth inhibition) was added to the trypsin solution before the incubation time. The inactivation dose of AD-associated bacterial was determined by exposing aliquots of the fresh prepared bacterial suspension (10^4 CFU in saline solution) to series doses of gamma irradiation (1, 1.5, 2, 2.5, and 3 KGy). The minimal irradiation dose that causes zero growth of bacteria was considered as the inactivation dose. Next

day, the denuded amnion fragments and bacterial planktons were discarded by centrifugation at 4000 rpm for 15 min. The supernatant was sterilized by gamma irradiation at dose 25 KGy. This supernatant contains 20% (w/v) soluble digested extract of amnion (because each 1 gm was digested into 5 ml) which abbreviated as IAME (irradiated amniotic membrane extract), and stored at 4 ^{o}C until using it in the subsequent experiments (up to 6 months). The irradiation process was performed in NCRRT (EAEA, Cairo) using Gamma cell-220 Excel Cobalt-60 irradiation Canadian facility. The dose rate at the time of the experiment was ~0.76 KGy/h.

Microbiological assessments

1. Antibacterial evaluation of preparations

The nanoparticles of ZnO (ηZnO) were purchased from Sigma-Aldrich (catalog number 677450), with diameter less than 50 nm. The antibacterial potentiality of ηZnO was assessed preliminary by evaluating three concentrations (1mM, 3mM and 5mM), in sodium chloride saline solution, against the grown bacteria in the swab culture. The least concentration, that revealed effective bactericidal activity, will be selected to be used for the subsequent experiments.

Filter-paper disc preparations of ηZnO and IAME were evaluated against all the selected MDR isolates. The discs were prepared by loading 10 ul of ηZnO or IAME onto a 6 mm-sterile filter-paper disc. Then, the loaded discs were left 10 min for air drying under laminar air flow to ensure full aseptic conditions.

All multidrug-resistant (MDR) bacterial isolates were sub-cultured in Tryptone Soya Broth (TSB) and incubated at 35°C for 18 h. Fresh bacterial suspensions were uniformly inoculated onto Mueller–Hinton Agar (MHA) plates using sterile cotton swabs to achieve a confluent lawn, following standard Clinical and Laboratory Standards Institute (CLSI) disk diffusion guidelines **[27]**. Plates were allowed to dry for 15 min at ambient temperature to facilitate inoculum absorption. Subsequently, prepared filter-paper disks impregnated with the respective test formulations were placed tightly onto the agar surface. Each 90 mm culture plate received six disks (comprising three replicate disks per treatment condition) to evaluate antimicrobial activity in triplicate ($n = 3$). Following incubation at 35°C for 24 h, the diameters of the resulting inhibition zones were measured in millimeters (mm) using a digital caliper and expressed as the mean $\pm$ standard deviation.

2. Determination of minimal inhibitory concentration (MICs)

The minimal concentration of ηZnO and IAME preparations that could inhibit the bacterial growth of the identified MDR strains is defined as MIC. Serial dilutions of each preparation were done ranged from 10 to 125µl/ml from the mother suspension (3 mM ηZnO or 20% IAME), in a 96-well microtitre plate. The concentration of the combination treatment was adjusted to be 1:1 from both preparations, and its dilutions were also ranged from 10 to 125µl/ ml. All dilutions were done in TSB medium. Each well contained the assigned dilution in 80 ul TSB medium, 10 ul bacterial inoculum (2×10^5 CFU/ml), and 10 ul Resazurin reagent (cell growth indicator) **[33]**. All

treatments were done in triplicates to evaluate according to the average. The experimental controls were assigned as; Negative controls represented the non- inoculated wells, and non-treated controls represented wells of non-treated cultures. The incubation was set at 37 °C for 18–24 h. Then, the color change was then assessed visually, as changes from purple to pink or colorless were recorded as positive indications.

3. Synergy testing

The fractional inhibitory concentration (FIC) index, of both antimicrobial agents (ηZnO and IAME) at the MIC value, was assessed to evaluate the synergy between their combinations by the checkerboard method **[34]**. The calculation of FIC was according to the following formulas:

$$FIC\ (\eta\mathrm{ZnO}) = \frac{MIC_{\eta\mathrm{ZnO}\ +IAME}}{MIC_{\eta\mathrm{ZnO}}} \longrightarrow (1)$$

$$FIC\ (IAME) = \frac{MIC_{\eta\mathrm{ZnO}\ +IAME}}{MIC_{IAME}} \longrightarrow (2)$$

$$FIC\ (index) = (1) + (2)$$

Combinations were classified as; synergistic, when the value of the FIC index (FICI) was ≤0.5, additive (>0.5 - ≤1.0), indifferent (>1.0 - ≤2.0), and antagonistic (>2.0).

4. Bacterial biofilm formation assay

Each identified bacterial species were represented by one isolate that showed the highest MIC value (the strongest resistant) for biofilm formation test, using optical density (OD) assessment of stained biofilms with crystal violet **[35]**. Briefly, each fresh-prepared culture in Tryptone Soya Broth (TSB), inoculated with 10^6 CFU/ml, was dispensed in triplicates as 0.2 ml per well in a flat-bottom microtiter plate (96-well), and incubated at 37°C for 48 hours. Then, the wasted media were aspirated from each well carefully to avoid damaging of the adhered biofilm in the bottom of the well. Then, the plate was washed two times with sterile phosphate buffer gently, and the biofilm was fixed to the bottom surface by incubation at 37°C for 1 h, and then stained by adding 0.1 ml of 0.1% crystal violet solution. The staining condition was adjusted at 37°C for 5 min **[36]**. the excessive stain was washed out twice with phosphate solution before the determination of the optical density of the biofilm at 570 nm wavelength, using Microplate Reader-Infinite M Nano 200 Pro. The obtained values of each bacterial strain were then averaged. Biofilm

intensity was classified as weak (OD range = 0.139- 0.276), moderate (OD range = 0.277- 0.414) and strong (OD >0.415).

The ability of bacteria to form a biofilm in the presence of ηZnO and IAME preparations was assessed similarly but with adding each preparation to the culture medium at the concentration of MIC (as determined above). The negative control was assigned in the wells contain cultures without any treatment.

5. Scanning electron microscopic analysis

Morphological alterations induced on the bacterial cell surface by the treatment with the co-formulation of ηZnO and IAME (Conc= MIC) were evaluated using scanning electron microscopy (SEM) and compared against untreated control cells. Briefly, freshly prepared bacterial cultures were exposed to the combination treatment and incubated for 18 h at 37 °C. Following incubation, bacterial cells were harvested by centrifugation at 4,000 rpm ($1{,}500 \times g$) for 15 min. The supernatant was discarded, and the cell pellet was washed twice with sterile phosphate-buffered saline (PBS, pH 7.4). The cells were fixed in a 2.5% (v/v) glutaraldehyde solution for at least 10 h at 4 °C. Subsequently, the fixed cells were collected and dehydrated through a graded ethanol series (30%, 50%, 70%, 80%, 90%, and 100% v/v in water). Finally, the bacterial suspension in 100% ethanol was mounted onto glass coverslips, allowed to air-dry, sputter-coated with a thin gold layer under vacuum, and examined using a ZEISS EVO 15 scanning electron microscope (Carl Zeiss Microscopy GmbH, Oberkochen, Germany) **[37]**.

Cytotoxicity assay

The biocompatibility of the prepared anti-bacterial formulations was evaluated referring to the cytotoxicity testing (according to ISO 10993-5). The cytotoxicity profile of IAME, ηZnO, and their combination (IAME : ηZnO = 1:1), across a concentration range of 10 to 125 μL/mL (around the obtained MIC values), was evaluated on human fibroblast normal cell line HFB4 (BBRJ code: nh-skp-fb0040, obtained from VACSERA's Tissue Culture Unit) **[38]**. The cellular response was measured as **Cell Viability (%)** and complementary **Cytotoxicity (%)**, where:

$$\text{Cytotoxicity (\%)} = 100\% - \text{Viability (\%)}$$

The measuring of cellular viability was based on the ability of vital cells to form Formazan crystals during the incubation with MTT (*3-(4,5-dimethylthiazol-2-yl)-2,5-diphenyltetrazolium bromide*) through mitochondrial enzymatic activity. Practically, in a 96-well plate, HFB4 cells were seeded with complete Dulbecco's Modified Eagle Medium (DMEM). Each well contained 100 μL total volume of liquid culture. The culture was incubated 24 hours at 37 ^{0}C with 5% CO_2 to let cells for complete adherence to the plate surface. Next day, the consumed medium was replaced with fresh medium contained the assigned concentration of treatment with IAME, ηZnO,

or their combination. Additional 24 hours of incubation was set at 37 ^{0}C. Next day, the consumed medium was replaced with fresh medium contained 10 µl of MTT stock solution (5 mg/ ml in PBS). After incubation at 37ºC for 4 hours, the reaction media was discarded and replaced with 100µl DMSO as a Formazan solubilizing solvent. The quantification of the purple color intensity of the formed Formazan in the viable cells was assessed by optical density measurement at a primary wavelength of 570 nm, where the background reference wavelength was set at 630 nm to eliminate optical noise **[39]**. The calculation of cellular viability percentage was done using the following equation:

$$\text{Cell Viability (\%)} = \left(\frac{\text{Absorbance}_{\text{treated sample}} - \text{Absorbance}_{\text{blank}}}{\text{Absorbance}_{\text{control}} - \text{Absorbance}_{\text{blank}}}\right) \times 100$$

The cytoprotective effect of IAME was referred to the calculation of **Cytotoxicity Mitigation Efficiency (ME)**, defined as:

$$\text{Mitigation Efficiency (\%)} = \left(\frac{\text{Cytotoxicity}_{\eta\text{ZnO}} - \text{Cytotoxicity}_{\text{Combo}}}{\text{Cytotoxicity}_{\eta\text{ZnO}}}\right) \times 100$$

All data were structured and processed using **scipy [40] and matplotlib [41]**. Statistical metrics computed included:

- **Descriptive Statistics**: Mean, standard deviation (SD), and standard error of the mean (SEM).
- **Linear Regression Analysis**: To model the concentration-response relationship of ηZnO and compute the half-maximal inhibitory concentration (IC_{50}).
- **Comparative Hypothesis Testing**:
    - **One-Way Analysis of Variance (ANOVA)** across all treatment agents.
    - **Paired Samples t-Test** to compare cytotoxicity levels between ηZnO alone versus ηZnO + IAME (combo).
- **Unified Analysis:** the Integration of Cell Viability (represented on left Y-axis) and Cytotoxicity Dose-Response Profiles (represented on right Y-axis) was visualized in a unified chart across all evaluated concentrations (10 to 125 μL/mL) on human fibroblast cells. When cell viability curve declines, cytotoxicity rises at an identical rate, so the **Intersection Point** between them at the 50% horizontal line represented IC_{50}value.

Anti-inflammatory assay

The potential anti-inflammatory of the test agents—Diclofenac sodium solution (as a standard drug, mother concentration = 1 mg/mL), IAME, ηZnO, and their 1:1 combination (ηZnO + IAME)—was quantified using a modified Bovine Serum Albumin (BSA) heat-induced denaturation assay **[42]**. Briefly, 50 μL of each treatment at serial concentrations (5–200 μL/mL) was mixed with 450 μL of a 1% w/v aqueous BSA solution. The reaction pH was adjusted to 6.3 ± 0.1 using 1 N HCl. Reaction mixtures were incubated at room temperature for 20 min, followed by thermal denaturation at 55°C for 30 min in a regulated water bath. After cooling to room temperature, absorbance (OD) was measured spectrophotometrically at 670 nm (Biosystem 310 Plus). Dimethyl sulfoxide (DMSO) served as the vehicle control. The percentage inhibition of protein denaturation was computed as:

$$\text{Inhibition (\%)} = \left[\frac{\text{OD}_{\text{Control}} - \text{OD}_{\text{Sample}}}{\text{OD}_{\text{Control}}}\right] \times 100$$

All assays were executed in triplicate ($n = 3$), and values are expressed as Mean $\pm$ Standard Deviation (SD) and Standard Error of the Mean (SEM). Concentration-response curves were modeled using four-parameter non-linear logistic regression to calculate half-maximal inhibitory concentrations (IC_{50}). Statistical significance across concentrations and treatment groups was evaluated using One-Way Analysis of Variance (ANOVA) followed by Tukey's *post-hoc* test ($p < 0.05$).

Antioxidant activities assay

The free-radical scavenging capacity of ηZnO, IAME, their 1:1 combination (ηZnO + IAME), and ascorbic acid (standard reference) was evaluated using the 2,2-diphenyl-1-picrylhydrazyl (DPPH) radical scavenging assay **[43]**. Reaction mixtures contained serial concentrations (25 to 200 μL/mL) of the respective test interventions mixed with DPPH solution. The mixtures were incubated in the dark for 30 min at 27 ºC. Then, the optical density (OD) was measured spectrophotometrically at 517 nm against a blank containing zero treatment concentration. The percentage of DPPH radical scavenging activity was determined as:

$$\text{DPPH Scavenging Activity (\%)} = \left[\frac{\text{OD}_{\text{Control}} - \text{OD}_{\text{Sample}}}{\text{OD}_{\text{Control}}}\right] \times 100$$

All experimental measurements were conducted in triplicate ($n = 3$), and values are expressed as Mean $\pm$ Standard Deviation (SD). Half-maximal inhibitory concentrations (IC_{50}) were calculated using non-linear log(inhibitor) vs. response regression analysis. Inter-group statistical differences across concentrations and treatments were analyzed using One-Way Analysis of Variance (ANOVA) followed by Tukey's *post-hoc* test ($p < 0.05$).

Results

Microbiological characterization of AD bacteria

All swabs (100%) that collected from the recruited AD patients showed positive microbial growth. All culture plates (n=30) represented 45 bacterial isolates. The re-cultivation of these isolates, separately on Mueller-Hinton Agar medium with antibiotic testing, showed that 33 out of 45 isolates (73.3%) are MDRs having antibiotic resistance ≥55.56% (**Table 1**). This highlighting high levels of multidrug resistance in the sample population.

Phenotypic and biochemical characterization differentiated a total of 33 MDR isolates and classified them into groups of similar characteristic isolates. All isolates were Gram-positive, catalase-positive cocci, confirming their identity as aerobic/facultative anaerobic skin-associated microflora while ruling out catalase-negative Streptococci **(Figure 1)**.

The modified oxidase (Microdase) test successfully differentiated micrococcal/kocurial flora from *Staphylococcus* species. Along with MALDI-TOF findings, a single isolate was identified as ***Kocuria rosea***, exhibiting a positive Microdase reaction, characteristic bright pink-to-red colony pigmentation, and lack of mannitol fermentation on Mannitol Salt Agar (MSA). Also, coagulase testing identified ***Staphylococcus aureus*****,** as a primary pathogen associated with AD lesions, from other *Staphylococcus* isolates. *S. aureus* isolates demonstrated positive coagulase activity, strong mannitol fermentation (yellow halos on MSA), and lipolytic activity on Baird-Parker agar (black colonies with clear halos due to egg yolk lecithinase cleavage). On the other hand, coagulase-negative staphylococci (CoNS) accounted for the remaining isolates were differentiated by trehalose fermentation and selective growth assays resolved these into three distinct CoNS species; *S. epidermidis*, *S. warneri*, and *S. hominis* (as confirmed by MALDI-TOF)**.**

S. epidermidis was identified as the primary CoNS colonizer, trehalose-negative and yielded small, pink-red colonies on MSA without mannitol utilization. While *S. warneri* and *S. hominis* were positive trehalose fermentation. Both of them were differentiated through the capability to ferment mannitol as a carbon source, where *S. warneri* isolates demonstrated rapid fermentation of mannitol yielding distinctive yellow color colonies, but *S. hominis* was weakly utilizing mannitol with typical small, non-pigmented colonies.

According to higher drug resistance (against antibiotics, ηZnO and IAME); 4 isolates of identified *S. aureus* (codes: 8, 11, 38, and 40), 4 isolates of *S. epidermidis* (codes: 2, 5, 22, and 34), 2 isolates of *S. warneri* (codes: 15, 43), 2 isolates of *S.hominis* (codes: 26, 41), and the only isolate of *Kocuria rosea* (code: 30) were selected as strong MDRs for the subsequent analysis**.**

On the other hand, the irradiation doses that caused growth inhibition for AD-associated bacteria were 2.5 and 3 KGy. Thus, the dose of 2.5 KGy was selected as the minimal inactivation dose. The addition of inactivated bacteria to the amniotic culture induced the amniotic cells to secret anti-microbial defense proteins in the culture medium. This caused the antibacterial activity of IAME.

Notably, the antibacterial activity of ηZnO was dose-dependent; the 1 mM concentration resulted weaker inhibition zones (faint) in the most culture plates than higher concentrations, but

no significant difference was recorded between 3 and 5 mM concentrations. Thus, the selected bactericidal formulation with minimal ηZnO concentration was 3 mM for the subsequent experiments.

Drug resistance profile

Generally, all isolated MDRs showed variable susceptibility to the anti-bacteria preparations of ηZnO and IAME. The mean inhibition zone diameter resulted by ηZnO ≈ 12.6 mm (**Range:** 8 mm – 17 mm), whereas the mean inhibition zone diameter resulted by IAME ≈ 16.8 mm (**Range:** 10 mm – 25 mm). Furthermore, IAME outperformed ηZnO in 32 of 33 isolates (96.97%), exhibiting larger inhibition zone diameters by an average of 3 to 8 mm.

In particular, isolates belonging to the same species exhibit near-identical susceptibility profiles, especially towards ηZnO and IAME. *Staphylococcus warneri* (isolates 15 & 43) demonstrated identical inhibition zone diameters for both ηZnO (10 mm) and IAME (12 mm), despite coming from different isolate codes and having slightly different antibiotic resistance percentages (66.6% vs. 55.5%). Also, *S. hominis* (Isolates 26 & 41) shared identical antibiotic resistance rates (55.5%) and ηZnO inhibition zones (8 mm), with minimal variation in IAME sensitivity (10 mm vs. 12 mm). whereas, *Staphylococcus epidermidis* demonstrated the highest average antibiotic resistance level among the identified species, as 3 out of 4 isolates (75%) possessed the maximum observed antibiotic resistance rate of **77.7%**, and were vulnerable to both ηZnO (8–10 mm) and IAME (10–12 mm). The results showed that ηZnO and IAME can effectively inhibit these major MDRs.

Quantitative evaluation of the MIC values revealed variable individual antimicrobial potencies between ηZnO and IAME across all 13 identified MDRs (**Table 2**). Individually, IAME exhibited superior intrinsic antibacterial activity compared to ηZnO, yielding a lower mean MIC of 63.46 ± 23.70 μl/ml (range: 37.5 to 100 μl/ml) versus 88.46 ± 26.65 μl/ml for ηZnO (range: 50 to 125 μl/ml). Notably, co-administration of ηZnO and IAME in a 1:1 combination resulted in a dramatic reduction in required inhibitory doses, bringing the mean combined MIC down to 16.15 ± 4.58 μl/ml (range: 12.5 to 25.0 μl/ml).

According to the classification framework established by **Yadav et al. (2013),** FICI values ≤ 0.5 denote synergistic interaction. All 13 tested isolates demonstrated unanimous synergism, with FICI values ranging from 0.25 to 0.5 (mean FICI $= 0.424 \pm 0.076$). The most profound synergistic effect was recorded in *S. hominis*, isolate 41 (FICI $= 0.25$), which achieved an 83.3% reduction in ηZnO MIC (FIC $= 0.1$) and an 85% reduction in IAME MIC (FIC $= 0.15$). Even highly resistant pathogens, such as *S. aureus* isolate 40 (displaying 77.7% baseline antibiotic resistance), exhibited marked synergistic susceptibility (FICI $= 0.325$), reducing single-agent MICs from 125 μl/ml (ηZnO) and 100 μl/ml (IAME) to 17.5 μl/ml in combination.

Comparative analysis across bacterial taxa highlighted both species-specific sensitivity baselines and universal susceptibility to dual-agent treatment (**Figure 2)**. Among the identified

species, *K. rosea* (isolate 30) demonstrated the highest baseline sensitivity to individual treatments (MIC $= 50\ \mu$l/ml for both ηZnO and IAME). Among the Staphylococcal species, *S. hominis* exhibited the lowest mean FICI (0.328 ± 0.110), followed by *S. aureus* (0.433 ± 0.075), *S. epidermidis* (0.444 ± 0.043), and *S. warneri* (0.451 ± 0.064).

Anti-biofilm treatment

Quantitative assessment of biofilm biomass using crystal violet assay ($OD_{570\ nm}$) demonstrated that single and combined treatments of ηZnO and IAME significantly reduced biofilm formation across all five representative bacterial isolates displaying high baseline MICs **(Figure 2)**. Untreated control cultures exhibited strong biofilm-forming capabilities, with optical densities ranging from 0.957 (*K. rosea*, isolate 30) to 1.530 (*S. aureus*, isolate 11). Monotherapy with ηZnO reduced biofilm formation by 51.7% to 74.2% (mean reduction: $66.06 \pm 8.78\%$), whereas single-agent treatment with IAME achieved biofilm reductions between 65.7% and 77.0% (mean reduction: $71.34 \pm 4.54\%$). Crucially, dual-agent administration (1:1 combination) elicited enhanced anti-biofilm activity across all tested strains, bringing mean optical density down to 0.160 ± 0.065 and achieving an overall mean density reduction of $86.34 \pm 4.63\%$. The highest degree of biofilm clearance was recorded in *K. rosea* 30 (92.0% reduction, $OD = 0.094$), followed by *S. hominis* 26 (89.0% reduction, $OD = 0.107$), *S. warneri* 43 (86.8% reduction, $OD = 0.140$), *S. aureus* 11 (84.3% reduction, $OD = 0.240$), and *S. epidermidis* 22 (79.6% reduction, $OD = 0.217$).

Microscopic evaluation of treatment

Morphological deformations were noted under SEM magnification due to the treatment with the dual-agent of ηZnO and IAME (1:1 combination), at the calculated concentration of the MIC value for each bacterial species. Compared to the normal control morphology, most treated cells showed partial lysis with initiated superficial damages (**Figure 3**). It is worth noting that this effect was happened within just 18 hours post-incubation with the treatment.

Biocompatibility of antimicrobial agents

As shown in Tables (3 and 4), IAME demonstrated biocompatibility across the entire tested spectrum (10 to 125 μL/mL). Dermal fibroblast viability remained essentially unaffected, ranging between 99.86% and 100% with an overall mean viability of $99.95 \pm 0.05\%$. Max cytotoxicity recorded for IAME was 0.141%, confirming that IAME possesses no intrinsic toxicity toward human fibroblast cultures.

On the other hand, ηZnO induced marked dose-dependent cell mortality. At 10 μL/mL, cytotoxicity was 25 %, escalating rapidly to 50 % at 25 μL/mL and reaching a peak cytotoxicity of 60.05% (39.95% viability) at 125 μL/mL. Linear regression fitting of ηZnO cytotoxicity across concentration (C) yielded:

$$\text{Cytotoxicity}_{\eta\text{ZnO}}(\%) = 0.2398 \cdot C + 34.8337 \quad (R^2 = 0.6632,\ p = 0.0485)$$

Then, the estimated half-maximal inhibitory concentration (IC_{50}) for ηZnO alone was calculated at 63.25 μL/mL. Co-treatment with IAME effectively shielded fibroblast cells against ηZnO-mediated toxicity ($p < 0.001$). Across all tested concentrations, cell viability in the combination group remained high and remarkably stable ($88.95\% - 91$ %, mean $89.79 \pm 0.70\%$). This indicated that the cytotoxicity was restricted to a narrow range ($9\ \% - 11.05\%$, mean $10.21 \pm 0.70\%$). The reduction in cytotoxicity achieved by IAME co-administration was 64 % **at** 10 μL/mL and surpassed 82 % at higher nanoparticle concentrations (≥ 75 μL/mL).

In harmony, the graphical analysis confirmed the obtained results from statistical analysis. The dual-panel graph (**Figure 4**) summarizes the cell viability trends (represented by solid lines with filled markers on the primary left Y-axis) and comparative cytotoxicity levels (represented by dashed lines with open markers on the secondary right Y-axis) across all tested concentrations. Significance markers indicate $p < 0.001$ relative to ηZnO alone. The treatment by IAME (**Green Trajectories**) showed that the viability curve remains flat along the 100% upper boundary, while the cytotoxicity curve rests along 0%, while ηZnO **(Red Trajectories)** showed a classic inverse crossover. As concentration increases from 10 to 125 μL/mL, cell viability sharply drops from 75% to 39.95%, while cytotoxicity rises proportionally from 25% to 60.05%. Then, the IC_{50} is represented at the intersection point of the viability and cytotoxicity curves where cross precisely at the 50% horizontal line. Linear regression estimates the IC_{50} threshold at 63.25 μL/mL. But, the co-administration of IAME **(Blue Trajectories)** prevents the progressive toxicity seen with ηZnO alone. Viability remains elevated at $\sim 90\%$ ($89.79 \pm 0.70\%$), while cytotoxicity is constrained to $\sim 10\%$ ($10.21 \pm 0.70\%$). Then, the **Cytoprotective Gap** is represented by the large vertical distance between the red dashed line (ηZnO cytotoxicity) and the blue dashed line ηZnO+IAME cytotoxicity) which highlights the 82.4% **reduction in nanoparticle toxicity** achieved by IAME ($p = 0.00053$).

Potential anti-inflammatory and antioxidant therapy

The anti-inflammatory activity of Diclofenac sodium, IAME, ηZnO, and their 1:1 combination (ηZnO + IAME) was evaluated using the heat-induced Bovine Serum Albumin (BSA) denaturation assay. All tested interventions exhibited concentration-dependent inhibition of protein denaturation across the evaluated range of 5 to 200 μL/mL ($p < 0.001$). The standard drug, Diclofenac sodium, demonstrated the highest potency, with an IC_{50} of 6.01 μL/mL and a

maximum inhibition of $93.80 \pm 0.43\%$ at $200\ \mu$L/mL. Among the novel test agents, single-agent IAME yielded moderate protection ($IC_{50} = 94.72\ \mu$L/mL), achieving $71.80 \pm 0.68\%$ denaturation inhibition at $200\ \mu$L/mL. In contrast, ηZnO monotherapy exhibited lower activity, requiring an IC_{50} of $175.40\ \mu$L/mL and capping at $53.00 \pm 0.26\%$ inhibition at the highest tested concentration. Notably, the 1:1 co-formulation (ηZnO + IAME) significantly enhanced protection relative to both single agents, shifting the concentration-response curve leftward to achieve an IC_{50} of $81.65\ \mu$L/mL and reaching $68.00 \pm 0.17\%$ maximal inhibition. Across lower-to-intermediate concentrations (5–100 μL/mL), the dual combination produced statistically significant additive protection over individual monotherapies ($p < 0.05$) (**Table 5, Figure 5**).

The free-radical scavenging capacity of ηZnO, IAME, their 1:1 combination (ηZnO + IAME), and standard Ascorbic Acid was assessed using the 2,2-diphenyl-1-picrylhydrazyl (DPPH) assay across serial concentrations (25 to $200\ \mu$L/mL). All tested interventions demonstrated a statistically significant, dose-dependent increase in DPPH radical neutralization ($p < 0.001$). Ascorbic Acid exhibited predictable high-potency radical clearance, yielding an IC_{50} of $17.14\ \mu$L/mL and achieving $90.00 \pm 3.00\%$ scavenging at $200\ \mu$L/mL. Among the single-agent formulations, IAME monotherapy demonstrated substantial antioxidant activity ($IC_{50} = 43.61\ \mu$L/mL), reaching $78.00 \pm 1.60\%$ clearance at the maximum tested concentration. Conversely, ηZnO monotherapy exhibited low intrinsic scavenging capacity ($IC_{50} = 302.15\ \mu$L/mL), peaking at only $35.00 \pm 1.00\%$ at $200\ \mu$L/mL. Remarkably, the 1:1 co-formulation (ηZnO + IAME) produced a potent leftward shift in the concentration-response curve, reducing the IC_{50} to $15.65\ \mu$L/mL and reaching a maximal scavenging capacity of $87.00 \pm 2.00\%$. At lower concentrations (25–100 μL/mL), the dual combination displayed statistically significant superior activity over both individual monotherapies ($p < 0.05$), effectively matching the free-radical neutralization profile of standard Ascorbic Acid (**Table 6, Figure 6**).

Discussion

Atopic dermatitis (AD) is a chronic, relapsing inflammatory skin disease characterized by severe epidermal barrier dysfunction, unmitigated cutaneous oxidative stress, dysregulated immune cascades, and high vulnerability to secondary microbial colonization. The pathogenesis of AD creates a self-perpetuating "itch-scratch" cycle where inflammation disrupts skin barrier lipids, increasing susceptibility to pathogenic biofilms, which further trigger inflammatory host responses. Consequently, effective therapeutic interventions must provide multi-targeted action combining broad-spectrum antimicrobial and anti-biofilm activity, potent antioxidant radical scavenging, and structural anti-inflammatory protection **[44,5]**.

The isolation and definitive species identification of *S. aureus*, *S. epidermidis*, *S. hominis*, *S. warneri*, and *K. rosea* directly from active AD hand lesions reinforce the critical role of cutaneous dysbiosis in maintaining local skin inflammation. Lesional skin on the hands is particularly vulnerable to mechanical abrasion, moisture loss, and environmental exposure, which compromise the stratum corneum and allow opportunistic staphylococci to transition from benign

commensals to persistent biofilm-forming pathogens. The presence of these multidrug-resistant (MDR), biofilm-producing strains on hand lesions directly correlates with severe local pruritus, epidermal scaling, and recalcitrant disease flare-ups **[45,46]**.

The core hypothesis of the present study was to achieve the therapeutic integration of antibacterial induced IAME—a bioactive matrix enriched with regenerative growth factors, extracellular components, and antimicrobial peptides—with zinc oxide nanoparticles (ηZnO). This co-formulation aims to establish multi-modal efficacy across all key pathological hallmarks of AD **[44,47]**. Opportunistic biofilm formation on lesional skin exacerbates AD severity by secreting enterotoxins and proteases that degrade the stratum corneum and perpetuate local inflammation **[5]**. Our findings demonstrate that combining ηZnO with IAME achieves significant biofilm clearance, reducing biomass density across resistant clinical skin isolates including *S. epidermidis*, *S. aureus*, and *S. hominis*. The nanostructured ηZnO disrupts bacterial cell membranes and matrix polymers, allowing the bioactive peptides within IAME to penetrate established biofilms **[18,19]**. By suppressing biofilm-associated persistence, the ηZnO + IAME formulation directly addresses the primary microbial trigger of AD flare-ups, effectively breaking the cycle of infection-driven skin barrier degradation **[5,19]**.

The intrinsic antibacterial activity of IAME is attributed to the secretion of antimicrobial peptides (AMPs) when amniotic cells undergo infection stimulation as an innate immune defense mechanism. Key among these defense proteins are cationic β-defensins, which exhibit broad-spectrum activity against bacteria, fungi, and enveloped viruses. These peptides electrostatically bind to negatively charged phospholipids, lipopolysaccharides (LPS), or teichoic acids on microbial cell membranes. Upon insertion into the lipid bilayer, they disrupt membrane integrity via pore formation or "carpet-like" lysis, leading to cytoplasmic leakage and cell death. Beyond direct membrane lysis, β-defensins bind and neutralize bacterial endotoxins to prevent excessive inflammatory cascades while stimulating epithelial cell proliferation and migration during tissue repair **[48]**. Previous research has established that human β-defensin 2 secretion is stimulated in amniotic cells during infection as a primary non-specific defense barrier **[25,48]**. Therefore, the present study utilized radiation-inactivated bacterial cells to simulate an artificial infection stimulus in amniotic tissue. Conversely, ηZnO exercises antibacterial activity through complementary mechanisms: mechanical cell wall disruption, generation of surface reactive oxygen species (ROS), and sustained release of Zn^{2+} ions **[20,21]**.

Notably, the degree of baseline resistance to conventional antibiotics (ranging from 55.5% to 77.7%) did not correlate with resistance or tolerance to ηZnO or IAME, confirming that these experimental agents act via distinct, non-overlapping biochemical pathways **[20,23]**. The universal synergy (FICI ≤ 0.5) observed across 100% of the tested cohort indicates a multi-target mode of action. Nanoparticle-induced disruption of outer bacterial membrane integrity by ηZnO likely facilitates enhanced cellular accumulation of IAME's bioactive defensins **[18,47]**. Statistically, this 1:1 co-formulation offers a 3- to 5.7-fold dose-sparing effect relative to single-agent administration. This substantial reduction in required concentration is clinically advantageous, as it significantly mitigates potential concentration-dependent nanoparticle cytotoxicity while

maximizing antimicrobial potency against recalcitrant multidrug-resistant pathogens **[20,23]**. By pairing the two compounds, effective bacterial inhibition is achieved at markedly lower individual dosages (e.g., reducing ηZnO requirements from 125 μL/mL to 12.5–25 μL/mL), thereby preventing toxic accumulation of nanomaterials in cutaneous applications **[20]**.

Comparative analysis across bacterial taxa highlighted both species-specific sensitivity baselines and universal susceptibility to dual-agent treatment. Among the identified species, *K. rosea* (isolate 30) demonstrated the highest baseline sensitivity to individual treatments (MIC = 50 μL/mL for both ηZnO and IAME). Among the staphylococcal species, *S. hominis* exhibited the lowest mean FICI (0.328 ± 0.110), followed by *S. aureus* (0.433 ± 0.075), *S. epidermidis* (0.444 ± 0.043), and *S. warneri* (0.451 ± 0.064).

All isolates exhibited robust biofilm-forming capacity, with baseline optical densities ranging from $OD_{570\,nm} = 0.957$ to 1.53. Biofilm-encased bacteria display heightened resistance to conventional therapeutics due to the physical diffusion barrier posed by extracellular polymeric substances (EPS) **[5]**. Consequently, the ability of the ηZnO + IAME co-treatment to attenuate biofilm formation—even among strains displaying elevated baseline MIC values—represents a significant therapeutic advancement. Mechanistically, this enhanced clearance stems from a complementary mode of action: ηZnO destabilizes EPS matrix components through localized ROS generation and physical disruption, facilitating the penetration and cellular accumulation of bioactive compounds in IAME **[18,19]**. Notably, the combination therapy achieved up to a 92.0% reduction in biofilm mass, providing substantial anti-biofilm activity while minimizing individual active concentrations. These findings confirm that combining ηZnO with IAME provides a viable strategy to suppress biofilm-associated microbial tolerance across multidrug-resistant staphylococcal and related Gram-positive isolates.

A paramount requirement for any topical formulation intended for compromised AD skin is a favorable therapeutic index combining high bio-functional activity with minimal dermal cytotoxicity **[47]**. While inorganic nanoparticles like ηZnO offer potent anti-biofilm capabilities, their clinical translational utility is frequently limited by concentration-dependent cytotoxicity toward mammalian skin cells, primarily mediated through intracellular ROS generation, membrane disruption, and mitochondrial dysfunction **[20,21]**.

The cytotoxicity assay results of this study demonstrate that IAME serves as an effective biological buffering agent against ηZnO-induced cell injury. The native matrix of IAME—enriched with regenerative cytokines, extracellular matrix components, and biological antioxidants—exhibits intrinsic biocompatibility and provides active cytoprotection to dermal fibroblasts **[48]**. When combined in the ηZnO + IAME (1:1) formulation, IAME suppresses nanoparticle cytotoxicity by $> 80\%$, shifting the overall safety profile and maintaining high cellular viability ($\approx 90\%$). This cytoprotection likely stems from the bio-functionalization or protein-capping of the ηZnO nanoparticle surface by IAME biomolecules, which quenches surface radical generation, prevents direct physical cell-membrane damage, and buffers intracellular oxidative stress **[20,21]**.

Cutaneous inflammation and protein denaturation further aggravate barrier disruption in AD lesions, leading to cellular degradation and auto-antigen presentation **[44]**. The ηZnO + IAME co-formulation demonstrated significant structural protein protection, lowering the median inhibitory concentration for heat-induced BSA denaturation to $IC_{50} = 81.65\ \mu$L/mL and outperforming individual monotherapies ($p < 0.05$). This anti-inflammatory activity is complemented by exceptional free-radical scavenging capacity ($IC_{50} = 15.65\ \mu$L/mL), which matched standard Ascorbic Acid ($IC_{50} = 17.14\ \mu$L/mL). Oxidative stress is a major driver of AD progression; reactive oxygen species damage epidermal lipids and amplify pro-inflammatory cytokine cascades **[44]**. The synergistic antioxidant effect observed here relies on the ηZnO core serving as an efficient electron-transfer scaffold, accelerating the radical-quenching capacity of bioactive molecules present in IAME **[18,47]**.

Numerous preclinical and clinical studies have demonstrated that soluble bioactive extracts derived from the amniotic membrane accelerate re-epithelialization, suppress inflammation, and promote tissue regeneration in various cutaneous lesions **[49]**. These regenerative properties are primarily driven by a rich composition of growth factors, anti-inflammatory cytokines, structural proteins, and antioxidant modulators. Key growth factors identified in amniotic derivatives include hepatocyte growth factor (HGF), transforming growth factor-beta (TGF-β), epidermal growth factor (EGF), fibroblast growth factors (FGFs), and keratinocyte growth factor (KGF). Furthermore, the anti-inflammatory and matrix-remodeling milieu features cytokines such as interleukin-6 (IL-6) and IL-8, along with essential extracellular matrix components including hyaluronic acid, collagen and fibronectin **[50]**. Additionally, the antioxidant capacity of these extracts is mediated by the regulation of cellular redox pathways, notably through the activation of the Nrf2/HO-1 defense axis **[51]**.

From a clinical translational perspective, these integrated results confirm the feasibility of the ηZnO + IAME co-formulation as a multi-target topical therapy for Atopic Dermatitis. Rather than relying on conventional single-target therapeutics or synthetic corticosteroids—which carry long-term risks such as epidermal atrophy—the combined formulation provides a non-steroidal, multi-functional approach. By simultaneously eradicating microbial biofilms, mitigating cytotoxicity, neutralizing cutaneous ROS, and suppressing protein denaturation-mediated tissue inflammation. Therefore, the ηZnO + IAME platform can restore the microenvironmental homeostasis required for epidermal repair and skin barrier regeneration to improve AD skin lesions **[44,47]**.

Conclusion

This study demonstrates the clinical feasibility, therapeutic efficacy, and biological safety of a novel 1:1 nano-bio-formulation combining induced bioactive IAME and ηZnO for potential managing Atopic Dermatitis (AD) hand lesions. By integrating the regenerative, cytoprotective matrix of IAME with the catalytic properties of ηZnO, the co-formulation achieves multi-targeted efficacy across the key pathological drivers of AD:

- **Pathogen Eradication:** Successfully degraded established biofilms formed by clinical AD hand MDR isolates (*S. aureus*, *S. epidermidis*, *S. hominis*, *S. warneri*, and *Kocuria rosea*), achieving up to 92.0% biomass reduction.
- **Anti-Inflammatory Protection:** Suppressed heat-induced protein denaturation ($IC_{50} = 81.65\ \mu$L/mL), significantly outperforming individual monotherapies in preserving structural protein integrity.
- **Potent Antioxidant Activity:** Exhibited exceptional free-radical scavenging capacity ($IC_{50} = 15.65\ \mu$L/mL), outperforming constituent single agents and matching standard Ascorbic Acid ($IC_{50} = 17.14\ \mu$L/mL).
- **Biocompatibility & Cytoprotection:** Co-administration with IAME attenuated ηZnO-induced cytotoxicity on human dermal fibroblasts by $> 80\%$, maintaining cell viability near 90%. Crucially, the cytotoxicity IC_{50} threshold of the combined formulation is substantially higher (>125 μL/mL) than its highest antimicrobial MIC value (25 μL/mL), anti-inflammatory IC_{50} (81.65 μL/mL), and antioxidant IC_{50} (15.65 μL/mL).

This wide therapeutic window confirms that the dual-therapy with ηZnO + IAME operates effectively at potent pharmacological doses well below toxic thresholds. By establishing a safe concentration profile without the risk of cytotoxic overdose, this dual nano-bio-formulation offers a safe, non-steroidal topical candidate capable of breaking the chronic "infection–inflammation–oxidative stress" cycle and supporting skin barrier restoration in AD hand lesions.

References

1. **Oh J, Kim S, Kim MS, Abate YH, Abd ElHafeez S, Abdelkader A, Abdi P, Abdulah DM, Aboagye RG, Abolhassani H, Abtahi D.(2025)** Global, regional, and national burden of asthma and atopic dermatitis, 1990–2021, and projections to 2050: a systematic analysis of the Global Burden of Disease Study 2021. The lancet respiratory medicine. May 1;13(5):425-46.
2. **Tegegnie AB, Mitiku YA, Alemu BW, Wollie YG, Alene T. (2025)** Magnitude of atopic dermatitis and associated factors among children in northwest Ethiopia. Scientific Reports. Jul 30;15(1):27882.
3. **Sharara, Z. (2026). Biologics in the treatment of atopic dermatitis. In M. S. Al Abadie (Ed.),** *Atopic dermatitis – Bridging the gap between clinical science and practical care*. IntechOpen.
4. **Chai H, Siu WS, Ma H, Li Y.(2025).** Understanding Atopic Dermatitis: Pathophysiology and Management Strategies. Biomolecules. Oct 24;15(11):1500.

5. **Geoghegan, J. A., Irvine, A. D., & Foster, T. J. (2018).** *Staphylococcus aureus* and atopic dermatitis: a complex interaction. *Trends in Microbiology*, 26(6), 484–497.

6. **O'Neill, J. (2016).** Tackling drug-resistant infections globally: Final report and recommendations. Review on Antimicrobial Resistance. Wellcome Trust & UK Government.

7. **World Health Organization. (2024).** *Global antimicrobial resistance and use surveillance system (GLASS) report: 2024*. World Health Organization.

8. **Ong, P. Y., Ohtake, T., Brandt, C., Strickland, I., Boguniewicz, M., Ganz, T., Gallo, R. L., & Leung, D. Y. (2002).** Endogenous antimicrobial peptides and skin infections in atopic dermatitis. *The New England Journal of Medicine*, 347(15), 1151–1160. https://doi.org/10.1056/NEJMoa021481

9. **Weidinger, S., & Novak, N. (2016).** Atopic dermatitis. *The Lancet*, 387(10023), 1109–1122. https://doi.org/10.1016/S0140-6736(15)00149-X

10. **Alexander, H., Paller, A. S., Traidl, S., Shivcuran, N. K., Clarke, M., & Flohr, C. (2020).** The role of bacterial, fungal, and viral infections in atopic dermatitis. *The Journal of Allergy and Clinical Immunology*, 146(5), 980–997. https://doi.org/10.1016/j.jaci.2020.09.020

11. **Biedermann, T., Skabytska, Y., Kaesler, S., & Volz, T. (2015).** Regulation of T cell immunity in atopic dermatitis by microbes: The good, the bad, and the ugly. *Immunological Reviews*, 268(1), 143–160. https://doi.org/10.1111/imr.12341

12. **Iwamoto, K., Moriwaki, M., Miyake, R., & Hide, M. (2019).** *Staphylococcus aureus* derives staphylococcal enterotoxin A to enhance baseline inflammation in atopic dermatitis. *Journal of Investigative Dermatology*, 139(11), 2382–2385. https://doi.org/10.1016/j.jid.2019.04.019

13. **Clausen, M. L., Agner, T., Lilje, B., Edslev, S. M., Johannesen, T. B., & Andersen, P. S. (2017).** Association of *Staphylococcus aureus* colonization with severity of atopic dermatitis, systemic inflammation, and skin barrier disruption. *JAMA Dermatology*, 153(12), 1263–1271. https://doi.org/10.1001/jamadermatol.2017.2910

14. **Simpson, E. L., Lio, P., Oh, C. W., & Eichenfield, L. F. (2021).** Antibiotic stewardship in dermatology: Minimizing resistance risks while optimizing patient outcomes in inflammatory skin disorders. *Dermatologic Therapy*, 34(2), e14810. https://doi.org/10.1111/dth.14810

15. **Hajar, T., Leshem, Y. A., Hanifin, J. M., Nedorost, S. T., Lio, P. A., Simpson, E. L., & Eichenfield, L. F. (2015). A systematic review of topical corticosteroid withdrawal**

("steroid addiction") in patients with dermatitis. *Journal of the American Academy of Dermatology*, 72(3), 541–549. https://doi.org/10.1016/j.jaad.2014.11.024

16. **Molly, A. E., Simpson, E. L., & Guttman-Yassky, E. (2020).** New and emerging therapies for atopic dermatitis. *The Lancet*, 396(10247), 345–360. https://doi.org/10.1016/S0140-6736(20)31286-0

17. **Paller, A. S., Kong, H. H., Seed, P., Naik, S., Scharschmidt, T. C., Gallo, R. L., & Luger, T. (2023).** The microbiome in atopic dermatitis: Pathophysiology and current target-specific therapeutic strategies. *Journal of Allergy and Clinical Immunology*, 151(4), 845–855. https://doi.org/10.1016/j.jaci.2023.01.012

18. **Applerot, G., Lellouche, J., Lipovsky, A., Nitzan, Y., Lubart, R., Gedanken, A., & Banin, E. (2012).** Understanding the antibacterial mechanism of wide bandgap metal oxide nanoparticles (ZnO and CuO). *Computers in Biology and Medicine*, 42(12), 1152–1162.

19. **Yusof, N. A. A., Zainal, Z., & Ahmad, S. A. (2023).** Antibacterial and antibiofilm potential of zinc oxide nanoparticles against multidrug-resistant skin pathogens. *Journal of Applied Microbiology*, 134(4), lxad072.

20. **Sirelkhatim, A., Mahmud, S., Seeni, A., Kaus, N. H. M., Ann, L. C., Bakhori, S. K. M., Hasan, H., & Mohamad, D. (2015). Review on zinc oxide nanoparticles: antibacterial activity and toxicity mechanism. *Nano-Micro Letters*, 7(3), 219–242.**

21. **Gudkov, S. V., Burmistrov, D. E., Serov, D. A., Rebezov, M. B., Semenova, A. A., & Lisitsyn, A. B. (2021).** A review of the antimicrobial properties of zinc oxide nanoparticles. *International Journal of Molecular Sciences*, 22(5), 2400.

22. **Espitia, P. J. P., Soares, N. F. F., Coimbra, J. S. R., de Andrade, N. J., Cruz, R. S., & Medeiros, E. A. A. (2012).** Zinc oxide nanoparticles: synthesis, antimicrobial activity and food packaging applications. *Food and Bioprocess Technology*, 5(5), 1447–1464.

23. **Alekish, M., Ismail, Z. B., & Saeed, M. (2024).** Synergistic antibacterial and antibiofilm activity of green-synthesized zinc oxide nanoparticles combined with bioactive plant extracts against clinical *Staphylococcus* isolates. *Microbial Pathogenesis*, 186, 106482.

24. **Kim, S., & Lee, J. (2025).** Effect of gamma irradiation on cellulose nanofibers. Journal of Wood Science, 71, article 37.

25. **Nemr, W., Bashandy, A.S., Araby, E. and Khamis, O. (2017)** Molecular displaying of differential immuno- response to various infections of amniotic epithelia.. Am. J. Reprod. Immunol. 77, e12662.

26. **World Medical Association. (2013).** World Medical Association Declaration of Helsinki: Ethical principles for medical research involving human subjects. *JAMA*, *310*(20), 2191–2194. https://doi.org/10.1001/jama.2013.281053

27. **Clinical and Laboratory Standard Institute recommendations (CLSI),** Performance Standards for Antimicrobial Susceptibility Testing, 17th informational supplement, Clinical and Laboratory Standards, Wayne, PA, **2007.**

28. **Holt, J.G., Krieg, N.R., Sneath, P.H., Safety, J.T. and Williams, S.T. (1993)** "Bergey's Manual of Determinative Bacteriology". Williams, K. and Wilkins, O. (Ed.), Baltimore, USA

29. **Boerlin, P., Kuhnert, P., Hüssy, D., & Schaellibaum, M. (2003).** Methods for identification of *Staphylococcus aureus* isolates in cases of bovine mastitis. *Journal of Clinical Microbiology*, *41*(2), 767–771.

30. **Isobe, R., Kaneko, K., Rikitomi, E., Tanaka, M., & Shimizu, A.** (2006). Development and evaluation of diagnostic tests for catalase production in bacterial identification. *Journal of Microbiological Methods*, 65(3), 512–518.

31. **Carroll, K.C., Pfaller, M.A., Karlowsky, J.A., Landry, M.L., McAdam, A.J., Patel, R. and Pritt, B.S. (eds) (2023)** Manual of clinical microbiology. 13th edn. Washington, DC: ASM Press.

32. **Radwan NK, Nemr W.** The use of irradiated amnion dressing for the treatment of antibiotic-disinfected skin ulcer. Journal of Tissue Engineering and Regenerative Medicine. 2020 Sep;14(9):1272-80.

33. **Sarker, S.D.; L. Nahar, Y. Kumarasamy**, **(2007)** Microtiter plate-based antibacterial assay in corporating resazurin as an indicator of cell growth, and its application in the in vitro antibacterial screening of phytochemicals, Methods 42 321–324.

34. **Yadav, M.K., Park, S.W., Chae, S.W., Song, J.J. and Kim, H.C. (2013).** Antimicrobial activities of Eugenia caryophyllata extract and its major chemical constituent eugenol against Streptococcus pneumoniae. Acta Pathologica,Microbiologica et Immunologica Scandinavica, 121(12), 1198–1206.

35. **Christensen, G.D., Simpson, W.A., Younger, J.J., Baddour, L.M., Barrett, F.F., Melton, D.M., Beachey, E.H. (1985)** Adherence of coagulase negative staphylococci to plastic tissue culture plates: a quantitative model for the adherence of staphylococci to medical devices. J. Clin. Microbiol. Dec. 22(6), 996-1006.

36. **Baldassarri, L., Simpson, W.A., Donelli, G., Christensen, G.D. (1993)** Variable fixation of staphylococcal slime by different histochemical fixatives. European journal of clinical microbiology & infectious diseases: Official Publication of the European Society of Clinical Microbiology, 12(11), 866–868.

37. **Dassanayake, R. P., Falkenberg, S. M., Stasko, J. A., Shircliff, A. L., Lippolis, J. D., & Briggs, R. E. (2020).** Identification of a reliable fixative solution to preserve the complex

architecture of bacterial biofilms for scanning electron microscopy evaluation. *PLOS ONE*, *15*(5), e0233973.

38. **Mendes, C., Thirupathi, A., Corrêa, M. E. A. B., Gu, Y., & Silveira, P. C. L. (2022).** The use of metallic nanoparticles in wound healing: New perspectives. *International Journal of Molecular Sciences*, *23*(23), 15376. https://doi.org/10.3390/ijms232315376

39. **Boonpisuttinant, K., Taka, T., Ruksiriwanich, W., Chutoprapat, R., Udompong, S., Kansawang, R., Sangsee, J., Chompoo, W., Samothai, K. and Srisuttee, R., (2023).** Assessment of in vitro anti-skin aging activities of Phyllanthus indofischeri Bennet extracts for dermatological and aesthetic applications. *Scientific reports*, *13*(1), p.18661.

40. **Virtanen, P., Gommers, R., Oliphant, T. E., Haberland, M., Reddy, T., Cournapeau, D., Burovski, E., Peterson, P., Weckesser, W., Bright, J., van der Walt, S. J., Brett, M., Wilson, J., Millman, K. J., Mayorov, N., Nelson, A. R. J., Jones, E., Kern, R., Larson, E., … SciPy 1.0 Contributors. (2020).** SciPy 1.0: Fundamental algorithms for scientific computing in Python. *Nature Methods*, *17*(3), 261–272. https://doi.org/10.1038/s41592-019-0686-2

41. **Hunter, J. D. (2007).** Matplotlib: A 2D graphics environment. *Computing in Science & Engineering*, *9*(3), 90–95. https://doi.org/10.1109/MCSE.2007.55

42. **Lopez-Miranda, J.L.; Molina, G.A.; González-Reyna, M.A.; España-Sánchez, B.L.; Esparza, R.; Silva, R.; Estévez, M.(2023)** Antibacterial and Anti-Inflammatory Properties of ZnO Nanoparticles Synthesized by a Green Method Using *Sargassum* Extracts. *Int. J. Mol. Sci.* , *24*, (2), 1474.

43. Sainakham, M., Jantrawut, P., Kiattisin, K., Chittasupho, C. and Singh, S., 2023. Potential of green extraction using edible deep eutectic solvents on the bioactivities from Curcuma aromatica rhizome extracts for food application. *Journal of Agriculture and Food Research*, *14*, p.100868.

44. **Bickers, D. R., & Athar, M.** (2006). Oxidative stress in the pathogenesis of skin disease. *Journal of Investigative Dermatology*, 126(12), 2565–2575.

45. **Kong, H. H., Oh, J., Deming, C., Conlan, S., Grice, E. A., Beatson, M. A., Nomicos, E., Polley, E. C., Komarow, H. D., Murray, P. R., Turner, M. L., & Segre, J. A.** (2012). Temporal shifts in the skin microbiome associated with disease flares and treatment in children with atopic dermatitis. *Genome Research*, 22(5), 850–859.

46. **Byrd, A. L., Belkaid, Y., & Segre, J. A.** (2018). The human skin microbiome. *Nature Reviews Microbiology*, 16(3), 143–155.

47. **Mishra, P. K., Mishra, H., Ekielski, A., Talegaonkar, S., & Vaidya, B.** (2022). Zinc oxide nanoparticles in modern transdermal drug delivery systems for dermatological disorders. *AAPS PharmSciTech*, 23(6), 185.

48. **Eckert, T., Kesper, D. A., & Mylonas, I.** (2017). Human β-defensins in the fetal membrane and amniotic fluid: Expression patterns and biological functions during pregnancy and infection. *American Journal of Reproductive Immunology*, 77(6), e12662.

49. **Murphy, S. V., Skardal, A., Song, L., Vacanti, K., Soker, S., & Atala, A. (2017).** Solubilized amnion membrane hyaluronic acid hydrogel accelerates full-thickness wound healing. *Stem Cells Translational Medicine*, *6*(11), 2020–2032. https://doi.org/10.1002/sctm.17-0053

50. Fitriani, N., Wilar, G., Narsa, A. C., Mohammed, A. F. A., & Wathoni, N. (2023). Application of amniotic membrane in skin regeneration. *Pharmaceutics*, *15*(3), 748.

51. **Guo, M., Wu, K., Yang, M., Yin, Y., Li, Z., Wang, G., Sun, J., & Fan, H. (2025).** Bovine amniotic membrane with antioxidant and anti-inflammatory properties for the repair of alkali-burned corneas. Acta Biomaterialia, 201, 198–211.

Statements & Declarations

Funding

The authors declare that no funds, grants, or other support were received during the preparation of this manuscript.

Data availability

The datasets generated and/or analysed during the current study are available in the supplementary files.

Ethics Approval and Consent to Participate

All experimental protocols involving the use of human tissues and swabs were approved by the Ethics Committee of the National Center for Radiation Research and Technology (REC-NCRRT; IRB 00011179), Egyptian Atomic Energy Authority (EAEA), under approval number (F/5H/24). All methods were carried out in accordance with relevant guidelines and regulations (Declaration of Helsinki). Written informed consent was obtained from all human donors prior to tissue or swab collection.

Tables and Figures

Table 1: Resistance profile of the collected Atopic dermatitis-associated bacterial isolates to the tested antibiotics (n=9), Zinc oxide nanoparticles (ηZnO), and the irradiated amniotic membrane extract (IAME).

Isolate code	Antibiotic resistance (%)	ηZnO Inhibition Zone (mm)	IAME Inhibition Zone (mm)	Isolate code	Antibiotic resistance (%)	ηZnO Inhibition Zone (mm)	IAME Inhibition Zone (mm)
1	77.7	15	17	**24**	33.3	Non-MDR	
2	77.7	10	12	**25**	66.6	14	22
3	33.3	Non-MDR		**26**	55.5	8	10
4	77.7	13	18	**27**	55.5	13	18
5	77.7	8	10	**28**	55.5	13	16
6	55.5	14	20	**29**	55.5	15	18
7	44.4	Non-MDR		**30**	55.5	10	12
8	66.6	10	12	**31**	77.7	17	25
9	33.3	Non-MDR		**32**	77.7	15	22
10	33.3	Non-MDR		**33**	77.7	17	24
11	66.6	8	10	**34**	77.7	8	12
12	44.4	Non-MDR		**35**	66.6	14	20
13	44.4	Non-MDR		**36**	66.6	15	21
14	55.5	16	18	**37**	66.6	14	22
15	66.6	10	12	**38**	66.6	10	12
16	44.4	Non-MDR		**39**	66.6	15	21
17	44.4	Non-MDR		**40**	77.7	11	13
18	44.4	Non-MDR		**41**	55.5	8	12
19	33.3	Non-MDR		**42**	55.5	16	18
20	77.7	15	20	**43**	55.5	10	12
21	55.5	15	22	**44**	55.5	15	14
22	55.5	8	12	**45**	55.5	15	20
23	44.4	Non-MDR					

912 **Table 2:** Quantitative Minimum Inhibitory Concentration (MIC) and Fractional Inhibitory
913 Concentration Index (FICI) Data Summary for the identified bacterial isolates.

Identified isolates	Antibiotic resistance (%)	MICs				
		ηZnO (µl/ml)	IAME (µl/ml)	ηZnO & IAME (µl/ml)	Fold-Reduction in MIC*	FICI Value
S. epidermidis (Isolate 2)	77.7	75	50	12.5	4.0x	0.420**
S. epidermidis (Isolate 5)	77.7	100	75	17.5	4.3x	0.405**
S. epidermidis (Isolate 22)***	55.5	125	100	25	4.0x	0.450**
S. epidermidis (Isolate 34)	77.7	50	50	12.5	4.0x	0.50**
S. aureus (Isolate 8)	66.6	75	37.5	12.5	3.0x	0.496**
S. aureus (Isolate 11)***	66.6	125	100	25	4.0x	0.450**
S. aureus (Isolate 38)	66.6	75	75	17.5	4.3x	0.460**
S. aureus (Isolate 40)	77.7	125	100	17.5	5.7x	0.325**
S. warneri (Isolate 15)	66.6	75	37.5	12.5	3.0x	0.496**
S. warneri (Isolate 43)***	55.5	100	75	17.5	4.3x	0.405**
S. hominis (Isolate 26)***	55.5	100	75	17.5	4.3x	0.405**
S. hominis (Isolate 41)	55.5	75	50	12.5	4.0x	0.250**
Kocuria rosea (Isolate 30)***	55.5	50	50	12.5	4.0x	0.50**

914 * The fold reduction in MIC was calculated versus the strongest individual agent
915 **Indicates Synergism
916 ***Indicates the intraspecies selected isolate that have the highest MIC values to represent its species taxon

Table 3: *In Vitro* Cell Viability and Cytotoxicity Profile Across Treatments

Concentration (µL/mL)	IAME Viability (%)	ηZnO Viability (%)	ηZnO + IAME Viability (%)	ηZnO Cytotoxicity (%)	ηZnO + IAME Cytotoxicity (%)	Mitigation Efficiency (%)
10.0	100.00	75.00	91.00	25.00	9.00	64.00%
25.0	100.00	50.00	90.00	50.00	10.00	80.00%
50.0	99.95	48.95	88.95	51.05	11.05	78.36%
75.0	99.86	43.86	89.86	56.14	10.14	81.94%
100.0	99.91	40.91	89.51	59.09	10.49	82.24%
125.0	99.95	39.95	89.40	60.05	10.60	82.35%

Table 4: Descriptive & Inferential Statistics Across Experimental Groups. Paired t-test analysis against ηZnO (as a reference toxic agent) confirms a statistically significant reduction in its cytotoxicity when IAME is co-administered with it ($t = 7.87, p = 0.00053$).

Agent	Mean Viability (%) ± SD	Mean Cytotoxicity (%) ± SD	Min / Max Cytotoxicity (%)	One-Way ANOVA	Paired t-test vs ηZnO
IAME Extract	99.95 ± 0.05%	0.05 ± 0.05%	0.00%/0.14%	$F = 74.51$	$t = 9.46, p < 0.001$
ηZnO	49.78 ± 13.02%	50.22 ± 13.02%	25.00% /60.05%	$p = 1.62 \times 10^{-8}$	Reference
ηZnO + IAME	89.79 ± 0.70%	10.21 ± 0.70%	9.00%/11.05%	($p < 0.0001$)	$t = 7.87, p = 5.32 \times 10^{-4}$

Table 5: Inhibition of Heat-Induced BSA Denaturation by Test Formulations (Zinc oxide nanoparticles (ηZnO), and the irradiated amniotic membrane extract (IAME)) versus standard anti-inflammatory drug of Diclofenac Sodium.

Concentration (µL/mL)	Diclofenac Sodium (% Inhibition ± SD)	IAME Monotherapy (% Inhibition ± SD)	ηZnO Monotherapy (% Inhibition ± SD)	ηZnO + IAME Combination (% Inhibition ± SD)
Control (0)	0.00 ± 0.00	0.00 ± 0.00	0.00 ± 0.00	0.00 ± 0.00
5	$48.24 \pm 0.40^{*}$	5.10 ± 0.35	6.00 ± 0.17	$14.00 \pm 0.17^{\dagger}$
10	$56.54 \pm 0.35^{*}$	14.70 ± 0.68	12.00 ± 0.17	$23.00 \pm 0.17^{\dagger}$
25	68.90 ± 0.34	23.60 ± 0.35	19.00 ± 0.17	$32.00 \pm 0.26^{\dagger}$
50	79.20 ± 0.43	33.20 ± 0.35	26.00 ± 0.26	$39.00 \pm 0.17^{\dagger}$
75	$83.70 \pm 0.29^{*}$	42.30 ± 0.26	32.00 ± 0.17	$46.00 \pm 0.26^{\dagger}$
100	87.60 ± 0.26	51.80 ± 0.35	39.00 ± 0.17	$54.00 \pm 0.17^{\dagger}$
150	$91.10 \pm 0.35^{*}$	61.70 ± 0.26	46.00 ± 0.17	61.00 ± 0.26
200	93.80 ± 0.43	71.80 ± 0.68	53.00 ± 0.26	68.00 ± 0.17
IC_{50} (µL/mL)	**6.01**	**94.72**	**175.40**	**81.65**

$^{\dagger}p < 0.05$ indicates statistically significant enhancement of combination therapy over both individual monotherapies at low-to-mid concentrations (5–100 µL/mL).

Table 6: DPPH Radical Scavenging Activity (%) of Test Agents and Standard

Concentration (µL/mL)	ηZnO (% Scavenging ± SD)	IAME (% Scavenging ± SD)	ηZnO + IAME (% Scavenging ± SD)	Ascorbic Acid (% Scavenging ± SD)
25	12.00 ± 0.50	44.00 ± 0.30	$56.03 \pm 0.75^{\dagger}$	56.00 ± 1.00
50	16.00 ± 2.00	50.00 ± 2.00	$60.00 \pm 2.00^{\dagger}$	60.00 ± 2.50
75	20.00 ± 0.80	58.67 ± 0.50	$67.00 \pm 0.30^{\dagger}$	72.00 ± 2.40
100	25.00 ± 1.00	64.00 ± 0.20	$74.00 \pm 1.60^{\dagger}$	83.00 ± 1.20
150	32.00 ± 1.30	70.00 ± 0.30	81.00 ± 3.70	87.00 ± 2.70
200	35.00 ± 1.00	78.00 ± 1.60	87.00 ± 2.00	90.00 ± 3.00
IC_{50} (μL/mL)	**302.15**	**43.61**	**15.65**	**17.14**

Values represent Mean $\pm$ Standard Deviation (SD) of triplicates ($n = 3$). $^{\dagger}p < 0.05$ indicates statistically significant synergy/enhancement over individual monotherapies (ηZnO and IAME alone).

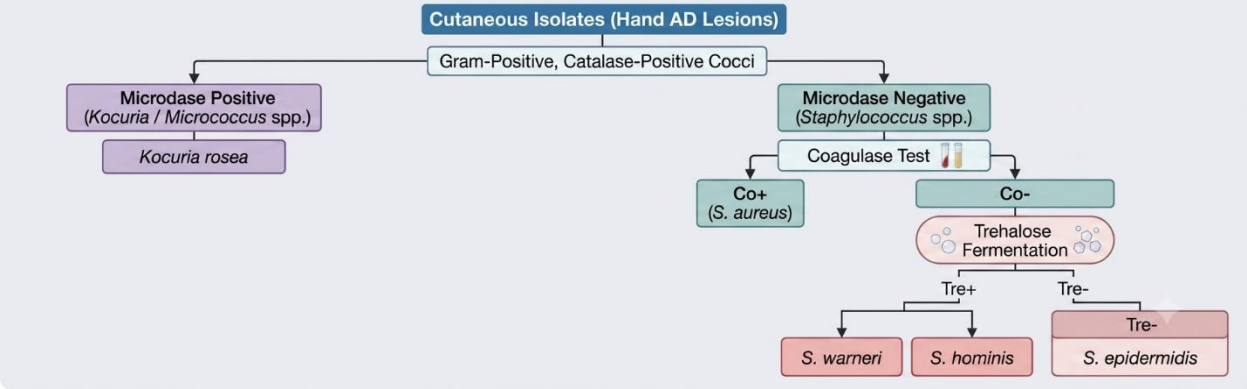


Figure 1: Biochemical identification schematic of skin-associated bacterial isolates from atopic dermatitis hand lesions. Sequential evaluation using Microdase, coagulase, and trehalose fermentation assays to differentiate *Kocuria rosea*, *Staphylococcus aureus*, and coagulase-negative staphylococci (*S. epidermidis*, *S. warneri*, and *S. hominis*).

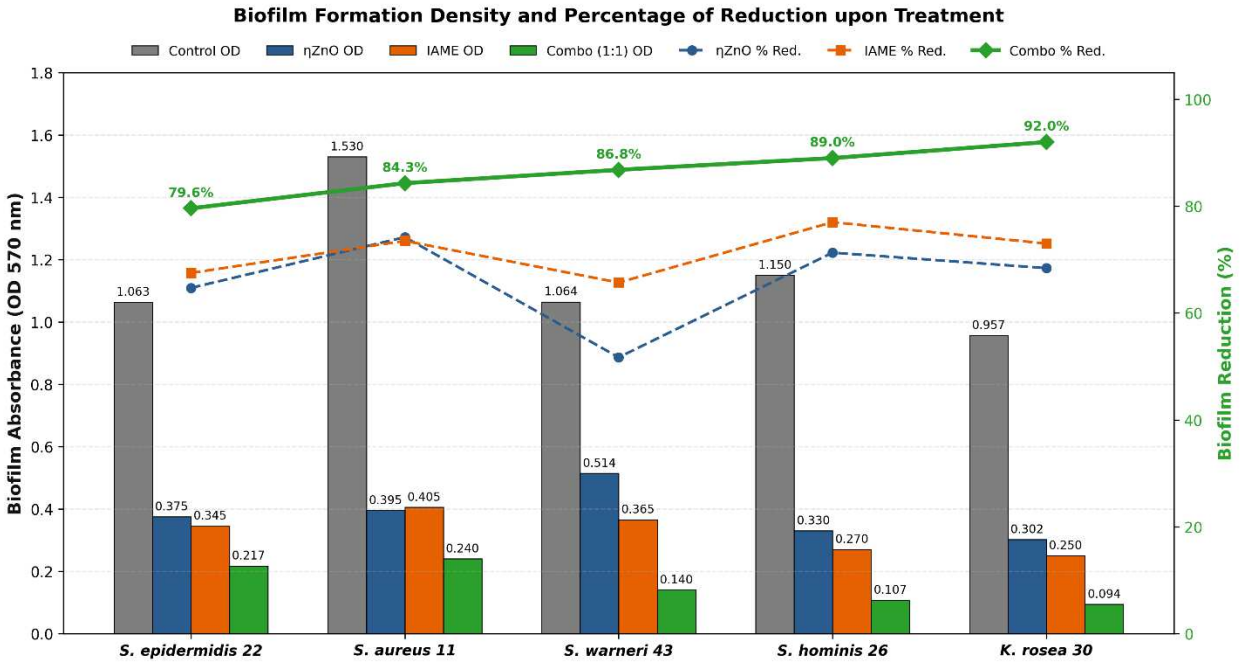
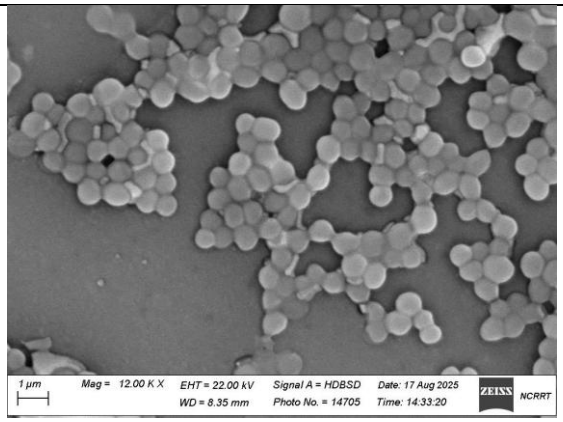
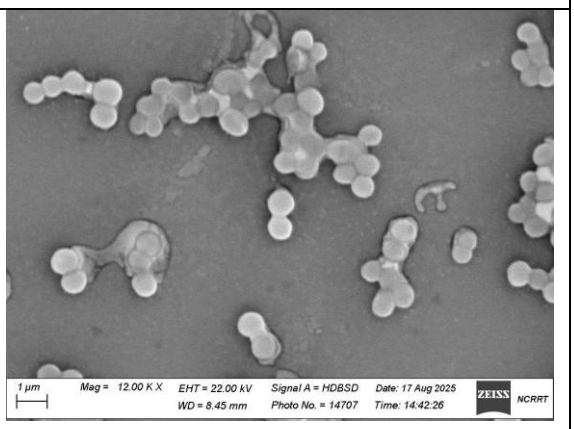
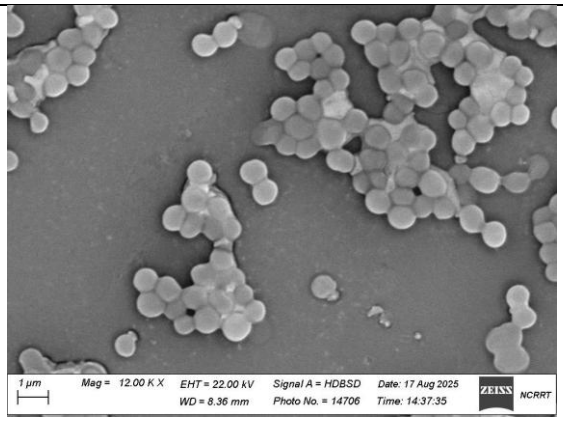
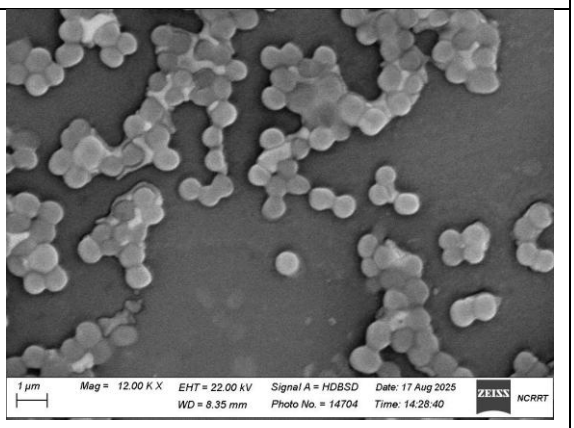
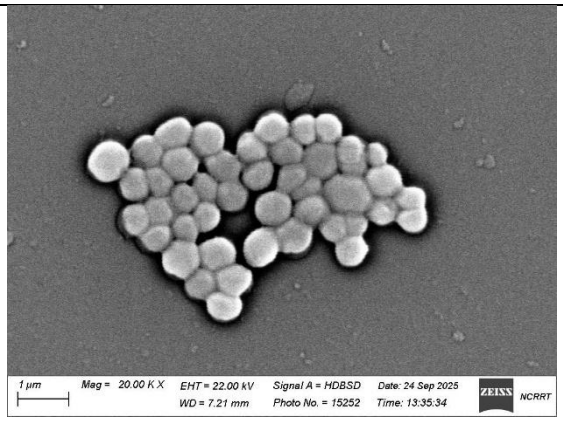
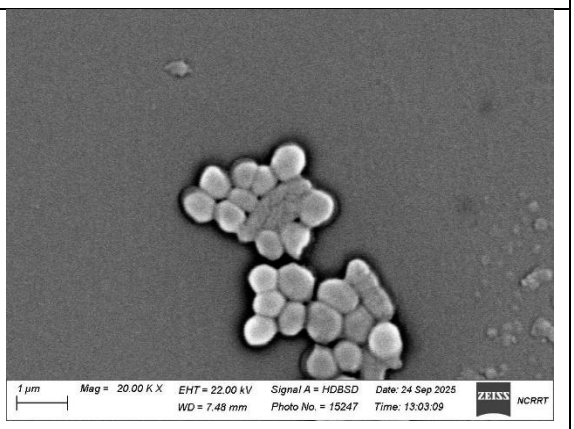


Figure 2: Quantitative evaluation of biofilm biomass and percentage of reduction upon the treatment across high-MIC isolates. Bar plots (left y-axis) represent raw biofilm density determined by crystal violet assay ($OD_{570\ nm}$) across control and single/combination treatment groups. Overlay lines (right y-axis) depict corresponding percentage reductions in biofilm density relative to untreated controls. Single-agent treatments (ηZnO and IAME) demonstrated moderate biofilm suppression, whereas dual-agent therapy (1:1 combination) achieved superior clearance across all tested strains, peaking at 92% inhibition in *Kocuria rosea* (isolate 30). Data values reflect mean absorbance measurements. (ηZnO: Zinc Oxide Nanoparticles; IAME: Irradiated Amniotic Membrane Extract; OD: Optical Density).

977

978

Strain	Non-treated	Combo-treated
S. epidermidis		
S. aureus		
S. warneri		

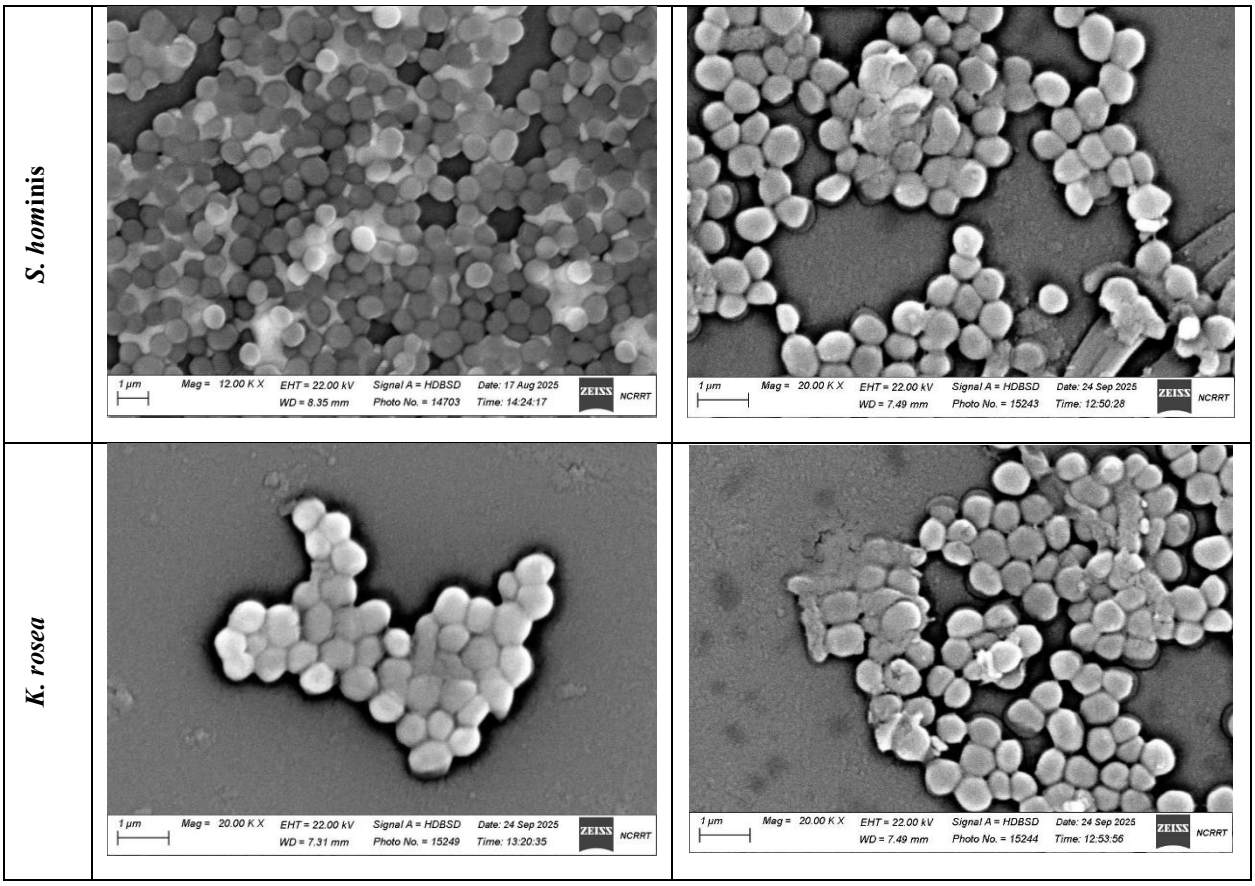


Figure 3: Scanning electron micrographs of the tested strains. The non-treated control appeared in normal morphology, whereas the treated cells with the combination of Zinc Oxide Nanoparticles and the Irradiated Amniotic Membrane Extract (Combo, 1:1) showed morphological deformations due to the lysis effect of the treatment.

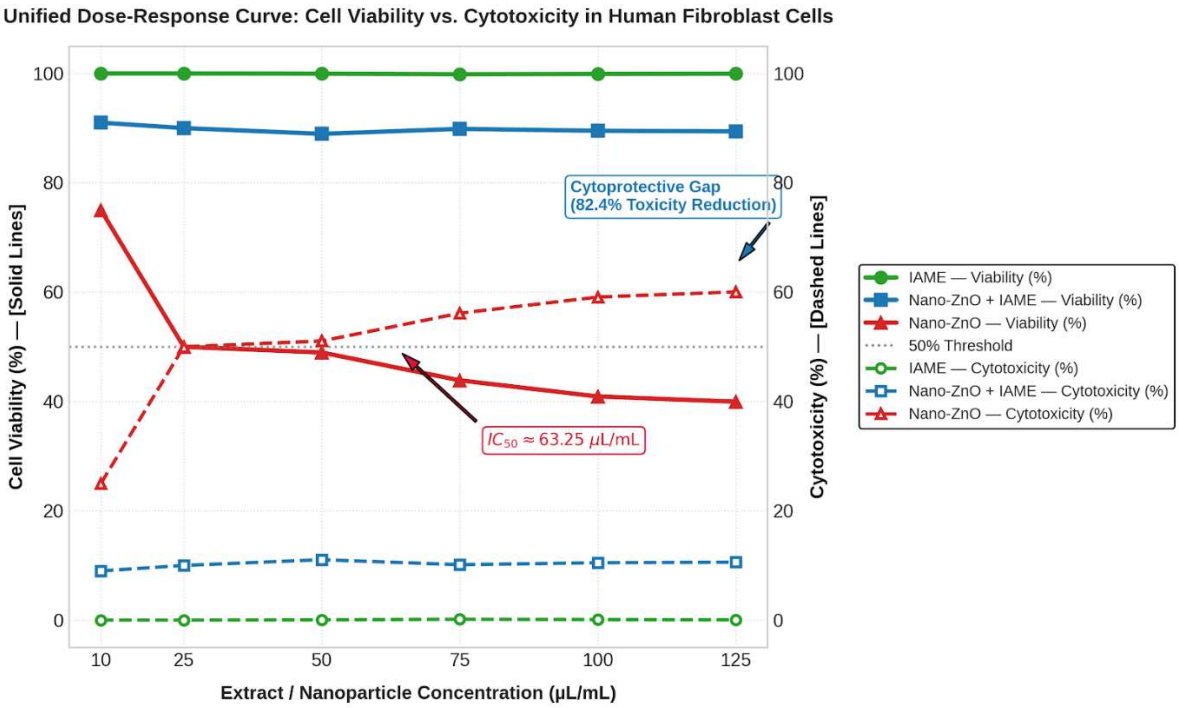


Figure 4: **Dose-Response Viability Curves and Comparative Cytotoxicity.** The dual-panel graph integrates both **Cell Viability (%)** (represented by solid lines with filled markers on the primary left Y-axis) and **Cytotoxicity (%)** (represented by dashed lines with open markers on the secondary right Y-axis) across all evaluated concentrations of Zinc Oxide Nanoparticles (**Nano-ZnO**) and the Irradiated Amniotic Membrane Extract (**IAME**) ($10 - 125\ \mu$L/mL); on human fibroblast cells.

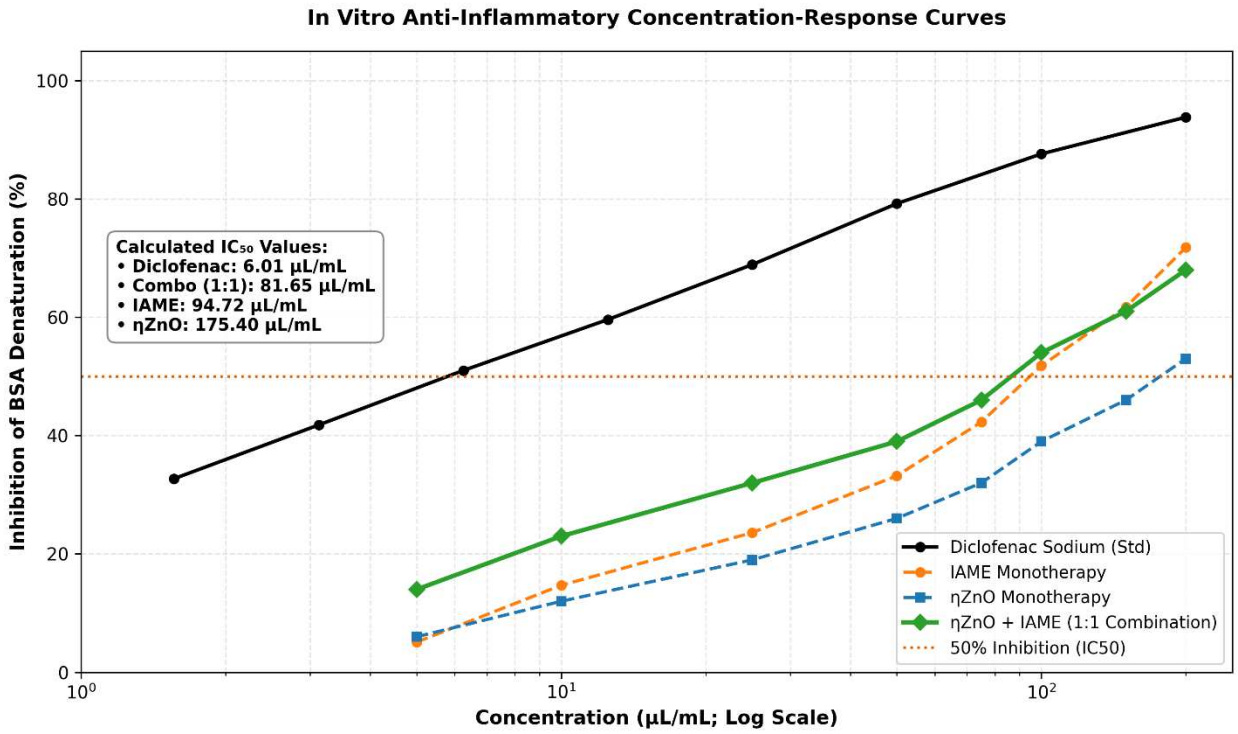


Figure 5: **Concentration-response anti-inflammatory activity and IC_{50} determinations in heat-induced bovine serum albumin (BSA) denaturation.** Semi-logarithmic concentration-response curves illustrating the percentage inhibition of thermal BSA denaturation across serial concentrations (5–200 μL/mL) of Diclofenac sodium (standard drug), IAME monotherapy, ηZnO monotherapy, and their 1:1 combination (ηZnO + IAME). The dashed horizontal line indicates the 50% inhibition threshold (IC_{50}). The dual combination (ηZnO + IAME) demonstrated superior anti-inflammatory potency ($IC_{50} = 81.65\ \mu$L/mL) compared to both individual interventions ($IC_{50} = 94.72\ \mu$L/mL for IAME and 175.40 μL/mL for ηZnO). Data points represent the mean $\pm$ standard error of the mean (SEM) of triplicate experiments ($n = 3$). (ηZnO: Zinc Oxide Nanoparticles; IAME: Irradiated Amniotic Membrane Extract; BSA: Bovine Serum Albumin).

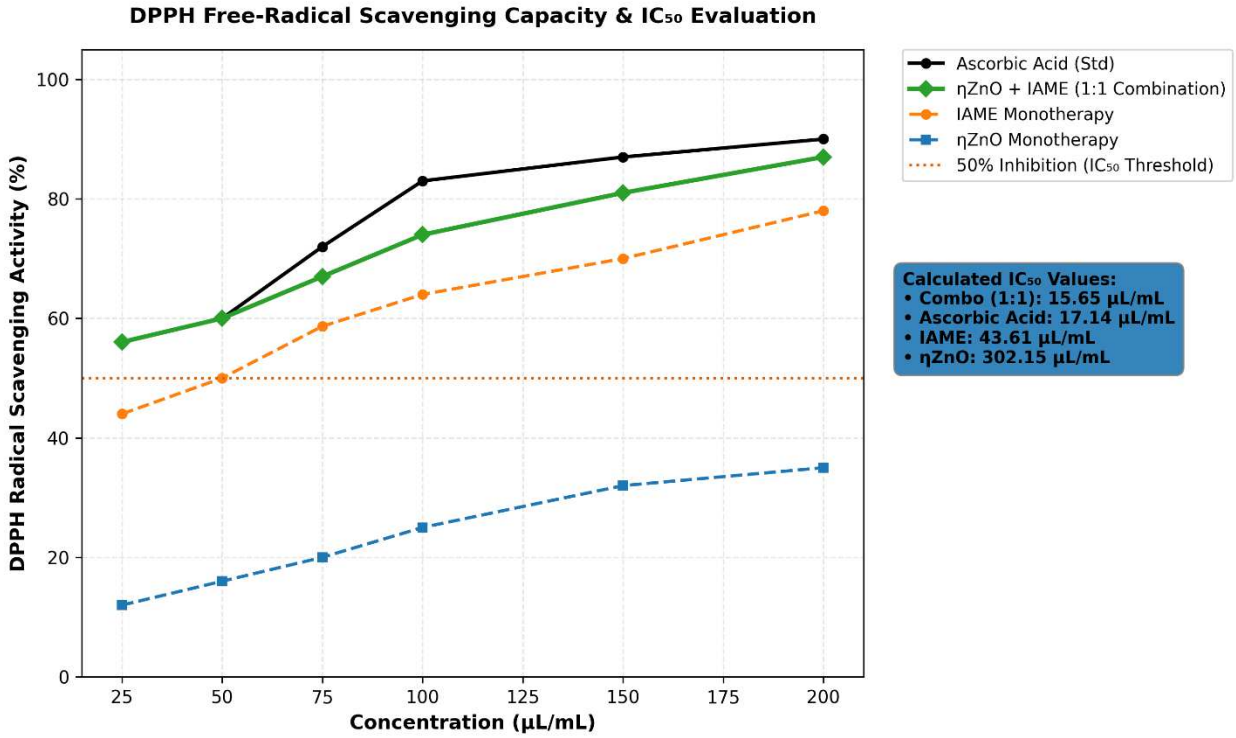


Figure 6: Dose-dependent DPPH free-radical scavenging capacity and IC_{50} determinations of test interventions relative to standard ascorbic acid. Concentration-response curves showing percentage DPPH radical clearance across serial concentrations (25–200 μL/mL) of ηZnO, IAME, their 1:1 combination (ηZnO + IAME), and Ascorbic Acid (positive control). The horizontal dotted line represents the median inhibitory threshold (50% scavenging). Co-formulation of ηZnO with IAME produced synergistic antioxidant activity ($IC_{50} = 15.65\ \mu$L/mL), surpassing individual constituent monotherapies ($IC_{50} = 43.61\ \mu$L/mL for IAME and 302.15 μL/mL for ηZnO) and matching the potency of standard Ascorbic Acid ($IC_{50} = 17.14\ \mu$L/mL). Data points denote the mean $\pm$ standard error of the mean (SEM) of triplicate measurements ($n = 3$). (ηZnO: Zinc Oxide Nanoparticles; IAME: Irradiated Amniotic Membrane Extract; DPPH: 2,2-diphenyl-1-picrylhydrazyl).

Supplementary Files

This is a list of supplementary files associated with this preprint. Click to download.

- Antiinflammatorytest.docx
- BiofilmTable.docx
- Cytotoxicityassay.docx
- AntioxidantTable.docx
- TablesofMIC.docx